Journal of Digital Imaging (2018) 31:799–850
https://doi.org/10.1007/s10278-018-0101-z

3D Segmentation Algorithms for Computerized Tomographic Imaging: a Systematic Literature Review

L. E. Carvalho[1,2] · **A. C. Sobieranski**[2,3] · **A. von Wangenheim**[1,2]

Published online: 18 June 2018
© Society for Imaging Informatics in Medicine 2018

Abstract

This paper presents a systematic literature review concerning 3D segmentation algorithms for computerized tomographic imaging. This analysis covers articles published in the range 2006—March 2018 found in four scientific databases (Science Direct, IEEEXplore, ACM, and PubMed), using the methodology for systematic review proposed by Kitchenham. We present the analyzed segmentation methods categorized according to its application, algorithmic strategy, validation, and use of prior knowledge, as well as its general conceptual description. Additionally, we present a general overview, discussions, and further prospects for the 3D segmentation methods applied for tomographic images.

Keywords 3D segmentation · Computerized tomographic imaging · Kitchenham's systematic review · Segmentation methods categorization

Introduction

Segmentation is a key process where a given input signal I is divided into its constituent regions or partitions [1]. These partitions should share some local properties in common regarding low-level cues, such as pixel or voxel intensities, continuity, and regularity of the signal, variance, texture information, and others, usually guided by some similarity criterion used to guide the merging process [2]. This basic concept goes beyond the idea of dimensionality and can be applied also to bi-dimensional or volumetric samples, single-channel or multi-variated real-domain, and multi-range or normalized data.

The early stages of image segmentation were derived from the uni-dimensional case of grayscale images. After several computational improvements of hardware architectures, those methods were quickly extended to the multi-dimensional case, including not only color but concatenating other information into subsequent dimensions. The fact is that there are several methods found in the literature whose concepts are merely extensions of the 1D case previously designed. Additionally, with the popularization of the use of volumetric data whose acquisition procedure is provided by a non-destructive device, such as computerized tomographic imaging—CT-imaging, magnetic resonance imaging—MRI, and its derivations; segmentation algorithms taking into account 3D information were also developed for health, material, geology, and many other application domains. Those methods are usually applied considering its voxel's organization in a fully 3D context, but can be applied slice by slice as well.

On the other hand, the wide variety of 3D segmentation methods can make difficult the analysis of the most suitable approaches for specific purposes/applications. Over the literature, we can find extensive reviews specifically designed to investigate 3D segmentation methods. For the medical context, there are several methods developed for the segmentation of specific human organs or anatomical structures. A more general description regarding 3D segmentation of medical images is presented by [3]. This review categorizes the segmentation methods into threshold, based on pattern recognition techniques and lastly deformable models. For each category typical algorithms are presented, as well as their potential applications for each model for female pelvic cavity. Later, the same authors present

✉ L. E. Carvalho
lcarvalho@incod.ufsc.br

[1] Graduate Program in Computer Science - Federal University of Santa Catarina, Florianopolis, Brazil

[2] Image Processing and Computer Graphics Lab - National Brazilian Institute for Digital Convergence - Federal University of Santa Catarina, Florianopolis, Brazil

[3] Department of Computing - Federal University of Santa Catarina, Ararangua, Brazil

a review of algorithms for medical image segmentation and their applications to female pelvic cavity [4], where the methods are classified into threshold-based, clustering-based, parametric, and geometric deformable model methods. The methods were tested for the segmentation of female pelvic cavity, presenting their distinct characteristics and presenting, in the end, the main observed guidelines for the construction of segmentation algorithms. In [5], a review of a total of 28 3D segmentation methods specifically designed to determine the composition of atherosclerotic plaques is presented. In this context, the morphology of atherosclerotic plaques need to be measured, besides other features such as echogenicity and texture found in images. The methods are categorized according to its main concept construction, such as image processing, clusterization, and supervised classification, as well as its effectiveness and drawbacks.

Different from the aforementioned studies, in this paper we aim to investigate and highlight the most relevant works over the literature, published within the range of 2006—March 2018, related to 3D segmentation considering CT-imaging as acquisition mean for general applications. Based on this investigation, we found several applications for 3D CT-imaging segmentation, as well as particular properties and features, that when analyzed collectively, categories of methods can be observed. This investigation has as main contribution the use of the guidelines proposed by Kitchenham [6], which is a well-established methodology for systematic literature review, providing a reproducible way to select relevant papers when the same keywords and tags are used.

The remaining of this paper is organized as follows: Section "Approach for Systematic Review of the Literature" describes a brief overview of the methodology applied to execute the systematic review of the literature. A general categorization of the 3D segmentation methods found in the literature is presented in "3D Segmentation Approaches". The performance evaluation and a general overview for 3D segmentation methods is described in "Performance Evaluation Analysis". Finally, discussion, future prospects and conclusions are presented in the "Discussion" and "Conclusion", respectively.

Approach for Systematic Review of the Literature

The Kitchenham's approach designed for systematic review has as main objective to provide a manner to evaluate and interpret all available research which is relevant to a particular research question, topic area, or phenomenon of interest [6]. Kitchenham's methodology is based on three guidelines used by medical researchers [7–10] and its most important feature is to keep the search reproducible when the same keywords and tags are used.

The following steps are executed to perform a systematic review of the literature as described by Kitchenham: first, a research topic is defined in order to guide the review process. In this paper, the research topic used was 3D segmentation applied to tomographic images. After defining the research topic, keywords and search tags are used to search papers on scientific databases. The following keywords and tags were used on the following scientific databases:

- Science Direct: *pub-date > 2005 and pub-date < March 2018 and TITLE-ABSTR-KEY(3D segmentation) and TITLE-ABSTR-KEY(computer tomography))*;
- IEEEXplore: *((“3D segmentation”) AND computer tomography) and Year: 2006 - March 2018)*;
- ACM: *((+“3D segmentation” +computer +tomography) and Published since: 2006 - March 2018)*;
- PubMed: *((“3D segmentation” AND full text[sb] AND (“2006/01/01”[PDat] : “2018/01/31”[PDat]))) AND Computer tomography;*

This search resulted on a total of 182 articles. The next step, is the articles selection based on a selection criterion. The following criterion was used in this work: articles written in the English language; having 3D segmentation algorithm as a main description, not only the use of a software that performs 3D segmentation; and the work was available for analysis, i.e., we had access to the full paper. With the selection criterion application, and removal of repeated works, 98 articles were selected, which required a detailed inspection. The selected works were categorized according to the main method used on the segmentation process. Finally, the Table 1 was constructed in chronological order, summarizing the highlighted works key aspects.

3D Segmentation Approaches

In this section we present the categorization of the selected works according to the main concept of construction employed. For each group of methods, a general description in terms of algorithmic functionality or strategy is provided.

The first group of methods are those based on simple segmentation techniques such as thresholding and graph-based approaches. As the input data is a volumetric information, the requirements for those methods are homogeneity and continuity verification based on voxel similarity. The next group of methods are based on curve or contour evolution, the so-called level set methods. These methods take the advantage of using gradient information to construct a vector field and then convolve a curve or

Table 1 Table summarizing the analyzed works

Autor(s)	Title	Year	Area	Method	A priori knowledge	Type of image	Category
Huang et al.	A TIGHTLY COUPLED REGION-SHAPE FRAMEWORK FOR 3D MEDICAL IMAGE SEGMENTATION	2006	Human Healthy	3D Markov Random fields and Deformable models	A priori object shape or seed points	Computed tomography	Model Based
Monga	Defining and computing stable representations of volume shapes from discrete trace using volume primitives: Application to 3D image analysis in soil science	2006	Geology	Region Growing based on graph	No	Computed tomography	Region Growing
Saragaglia et al.	Assessment of Airway Remodeling in Asthma: Volumetric Versus Surface Quantification Approaches	2006	Human Healthy	Deformable models, mathematical morphology and contours pairing based on energy calculation	No	Computed tomography	Model Based
Davis et al.	Assessment of 18F PET signals for automatic target volume definition in radiotherapy treatment planning	2006	Human Healthy	Threshold and region growing	Information of initial points belonging to the region of interest and to the background	Positron Emission Tomography	Region Growing
Nain et al.	A TIGHTLY COUPLED REGION-SHAPE FRAMEWORK FOR 3D MEDICAL IMAGE SEGMENTATION	2006	Human Healthy	Spherical wavelet functions	A priori object shape (training)	Magnetic Resonance Imaging	Model Based
Li et al.	Automatic clinical image segmentation using pathological modeling, PCA and SVM	2006	Human Healthy	Principal component analysis, level set and Support vector machine	Training	Computed tomography	Neural Network
Juslin et al.	Unsupervised Segmentation of Cardiac PET Transmission Images for Automatic Heart Volume Extraction	2006	Human Healthy	Markov Random Fields and Deformable Models	Prior knowledge about the heart positioning	Positron Emission Tomography	Model Based
Staal et al.	Automatic rib segmentation and labeling in computed tomography scans using a general framework for detection, recognition and segmentation of objects in volumetric data	2006	Human Healthy	Threshold, region growing and classification	Training	Computed tomography	Region Growing
Wieclawek et al.	Live-Wire-Based 3D Segmentation Method	2007	Human Healthy	Live-wire, wavelet and Fuzzy C-Means	Selection of a seed point to highlight a desired border	Computed tomography	Graph-Based

Table 1 (continued)

Autor(s)	Title	Year	Area	Method	A priori knowledge	Type of image	Category
Bulu et al.	Comparison of 3D Segmentation Algorithms for Medical Imaging	2007	Human Healthy	Four algorithms: region growing (one with seed points and the other without), Weibull E-SD Fields and an automatic multi-level thresholding using OTSU	Selection of seed points for the region growing algorithm	Computed tomography	Region Growing
Diciotti et al.	3-D Segmentation Algorithm of Small Lung Nodules in Spiral CT Images	2008	Human Healthy	Region growing and geodesic distance	Selection of a central voxel to delimit the volume of interest	Computed tomography	Region Growing
Jiamin Liu et al.	Rigid model-based 3D segmentation of the bones of joints in MR and CT images for motion analysis	2008	Human Healthy	live wire and volume matching	Selection of a seed point to highlight a desired border	Magnetic Resonance imaging and Computed Tomography	Graph-Based
D.Chen et al.	ACCURATE AND FAST 3D COLON SEGMENTATION IN CT COLONOGRAPHY	2009	Human Healthy	Threshold and adaptive level set function	Information of 4 initial seed points	Computed tomography	Level Set
D.Chen et al.	A variational framework for 3D colonic polyp visualization in virtual colonoscopy	2009	Human Healthy	Threshold and adaptive level set function	Information of 4 initial seed points	Computed tomography	Level Set

Table 1 (continued)

Autor(s)	Title	Year	Area	Method	A priori knowledge	Type of image	Category
Aslan et al.	SEGMENTATION OF TRABECULAR BONES FROM VERTEBRAL BODIES IN VOLUMETRIC CT SPINE IMAGES	2009	Human Healthy	Graph cut and region growing	Localization of the vertebral region	Computed tomography	Graph-Based
Ding et al.	3D Segmentation of Soft Organs by Flipping-Free Mesh Deformation	2009	Human Healthy	Deformable models	No	Computed tomography	Model Based
Chang et al.	A New 3D Segmentation Algorithm Based On 3D PCNN For Lung CT Slices	2009	Human Healthy	Neural Network model	Training	Computed tomography	Neural Network
H. JIANG et al.	Automatic 3D Segmentation of CT Images Based on Active Contour Models	2009	Human Healthy	Active contours and Threshold	No	Computed tomography	Model Based
K. Lai et al.	Automatic 3D Segmentation of Lung Airway Tree: A Novel Adaptive Region Growing Approach	2009	Human Healthy	Adaptive Region growing	No	Computed tomography	Region Growing
Hong Zhang et al.	3D SEGMENTATION OF THE LIVER USING FREE-FORM DEFORMATION BASED ON BOOSTING AND DEFORMATION GRADIENTS	2009	Human Healthy	Deformable models	A priori knowledge about intensity and shape	Computed tomography	Model Based

Table 1 (continued)

Autor(s)	Title	Year	Area	Method	A priori knowledge	Type of image	Category
Qian Wang et al.	Segmentation of Lung Nodules in Computed Tomography Images Using Dynamic Programming and Multi-direction Fusion Techniques	2009	Human Healthy	Dynamic programming modeling	Training	Computed tomography	Miscellaneous
Hong Zhang et al.	3D SEGMENTATION OF THE LIVER USING FREE-FORM DEFORMATION BASED ON BOOSTING AND DEFORMATION GRADIENTS	2009	Human Healthy	Deformable models	A priori knowledge about intensity and shape	Computed tomography	Model Based
Qian Wang et al.	Segmentation of Lung Nodules in Computed Tomography Images Using Dynamic Programming and Multi-direction Fusion Techniques	2009	Human Healthy	Dynamic programming modeling	Training	Computed tomography	Miscellaneous

Table 1 (continued)

Autor(s)	Title	Year	Area	Method	A priori knowledge	Type of image	Category
Bert et al.	An automatic method for colon segmentation in CT colonography	2009	Human Healthy	Threshold and Adaptive Region growing	Previous knowledge of threshold value appropriate for the application area	Computed tomography	Region Growing
Moussavi et al.	3D segmentation of cell boundaries from whole cell cryogenic electron tomography volumes	2009	Histology	Conditional random field associated with an inference process updated on each iteration	Labeling of the initial slice	Cryon-electron tomography	Model Based
Jun-Wei et al.	A Novel Automatic Extraction Method of Lung Texture Tree from HRCT Images	2009	Human Healthy	Level set, Active contour model guided by an energy functional	No	Computed tomography	Level Set
Y. h. REN et al.	A 3D Segmentation Method of Lung Parenchyma Based on CT Image Sequences	2010	Human Healthy	Adaptive thresholding, Connected component, region growing and morphological operators	No	Computed tomography	Region Growing
Hadjiiski et al.	Head and Neck Cancers on CT: Preliminary Study of Treatment Response Assessment Based on Computerized Volume Analysis	2010	Human Healthy	3D level set	Approximate bounding box for the lesion of interest	Computed tomography	Level Set
Hadjiiski et al.	Treatment Response Assessment of Head and Neck Cancers on CT Using Computerized Volume Analysis	2010	Human Healthy	3D level set	Approximate bounding box for the lesion of interest	Computed tomography	Level Set

Table 1 (continued)

Autor(s)	Title	Year	Area	Method	A priori knowledge	Type of image	Category
Aslan et al.	A NOVEL, FAST, AND COMPLETE 3D SEGMENTATION OF VERTEBRAL BONES	2010	Human Healthy	Graph cut and region growing	No	Computed tomography	Graph-Based
Gloger et al.	A fully automatic three-step liver segmentation method on LDA-based probability maps for multiple contrast MR images	2010	Human Healthy	Threshold, Region growing and probability map	Training	Computed tomography	Region Growing
Badakhshannoory et al.	A Model-Based Validation Scheme for Organ Segmentation in CT Scan Volumes	2011	Human Healthy	Principal component analysis and model construction	No	Computed tomography	Model Based
Cascio et al.	Automatic detection of lung nodules in CT datasets based on stable 3D mass-spring models	2011	Human Healthy	Region growing and deformable models	No	Computed tomography	Model Based
Bhole et al.	3D Segmentation in CT Imagery with Conditional Random Fields and Histograms of Oriented Gradients	2011	Human Healthy	Markov Random Fields, Conditional Random Fields and histograms for gradient orientation	User iteration for initial alignment	Computed tomography	Model Based
Shaoting Zhang et al.	3D Segmentation of Rodent Brain Structures Using Hierarchical Shape Priors and Deformable Models	2011	Human Healthy	Shape database segmentation	Training	Magnetic Resonance Imaging	Model Based

Table 1 (continued)

Autor(s)	Title	Year	Area	Method	A priori knowledge	Type of image	Category
De Nuzio et al.	Automatic Lung Segmentation in CT Images with Accurate Handling of the Hilar Region	2011	Human Healthy	3D Region growing	No	Computed tomography	Region Growing
Müller et al.	Model Based 3D Segmentation and OCT Image Undistortion of Percutaneous Implants	2011	Animal Healthy	Model based on Markov Random fields	Shape of the subcutaneous implants	Optical Coherence Tomography	Model Based
Kongkuo Lu et al.	Segmentation of the central-chest lymph nodes in 3D MDCT images	2011	Human Healthy	Border detection and optimal graph search with active contour analysis	Information of seed points	Computed tomography	Graph-Based
X. Chen et al.	3D Segmentation of Fluid-Associated Abnormalities in Retinal OCT: Probability Constrained Graph-Search-Graph-Cut	2012	Human Healthy	Search and cut in graph and voxel classification	Training	Optical Coherence Tomography	Graph-Based
Barbosa et al.	B-Spline Explicit Active Surfaces: An Efficient Framework for Real-Time 3D Region-Based Segmentation	2012	General objects	Minimization of energy functional	Definition of origin of the coordinate system	Computed tomography and Ultrasound	Model Based
X. Liu et al.	Fully Automatic 3D Segmentation of Iceball for Image-Guided Cryoablation	2012	Human Healthy	Graph cut	A priori knowledge about object shape	Computed tomography and Magnetic Resonance Imaging	Graph-Based
Spampinato et al.	Automatic 3D Segmentation of Mandible for Assessment of Facial Asymmetry	2012	Human Healthy	Connected component and bit-plane slice coding	Definition of the Region of interest	Computed tomography	Miscellaneous
Uher et al.	Automatic 3D Segmentation of Human Brain Images Using Data-mining Techniques	2012	Human Healthy	Region growing	Training	Computed tomography	Region Growing

Table 1 (continued)

Autor(s)	Title	Year	Area	Method	A priori knowledge	Type of image	Category
Urschler et al.	Forensic-Case Analysis: From 3D Imaging to Interactive Visualization	2012	Forensic analysis	Geodesic active contour and energy minimization in a variational framework	A priori knowledge about grayscale and texture values and shape restrictions	Computed tomography and Magnetic Resonance Imaging	Model Based
Shaoting Zhang	TOWARDS ROBUST AND EFFECTIVE SHAPE PRIOR MODELING: SPARSE SHAPE COMPOSITION	2012	Human Healthy	Shape database segmentation	Training	Computed tomography and Magnetic Resonance Imaging	Model Based
Li Zhang et al.	Automated Segmentation of the Choroid from Clinical SD-OCT	2012	Human Healthy	Hessian matrix analysis and thresholding	No	Spectral Domain Optical Coherence Tomography	Threshold
Loss et al.	Automatic Segmentation and Quantification of Filamentous Structures in Electron Tomography	2012	General objects	Tensor voting and Curve tracking	No	Electron 3D Tomography	Miscellaneous
Hutter et al.	Prior-Based Automatic Segmentation of the Carotid Artery Lumen in TOF MRA	2012	Human Healthy	Adaptive threshold and level set	A priori knowledge about irregular patterns of blood flow	Magnetic resonance Angiography	Level Set
Delibasis et al.	An Intelligent Tool for Anatomical Object Segmentation Using Deformable Surfaces	2012	General objects	Deformable models	Initial iteration for initialization of the active surfaces	Computed tomography	Model Based

Table 1 (continued)

Autor(s)	Title	Year	Area	Method	A priori knowledge	Type of image	Category
Lloréns et al.	Jaw tissues segmentation in dental 3D CT images using fuzzy-connectedness and morphological processing	2012	Human Healthy	Threshold and Fuzzy Connectedness Object Extraction	No	Computed tomography	Miscellaneous
Rüegsegger et al.	Statistical Modeling of the Eye for Multimodal Treatment Planning for External Beam Radiation Therapy of Intraocular Tumors	2012	Human Healthy	Statistical Modeling and Active shape model	Training	Computed tomography	Model Based
Reinhard Beichela et al.	Liver segmentation in contrast enhanced CT data using graph cuts and interactive 3D segmentation refinement methods	2012	Human Healthy	Graph-cut, chunk refinement and surface refinement	User iteration for refinement and seed point selection	Computed tomography	Graph-Based
Reinhard Beichela et al.	Liver segmentation in contrast enhanced CT data using graph cuts and interactive 3D segmentation refinement methods	2012	Human Healthy	Graph search problem solved by maximum flow algorithm	user defined lymph node approximate center and iterative refinement	Computed tomography	Graph-Based
Rusu et al.	Automated tracing of filaments in 3D electron tomography reconstructions using Sculptor and Situs	2012	Human Healthy	Genetic algorithms and stochastic searched based on templates	Initial points for the removal of regions without filaments	Cryon-electron tomography	Miscellaneous
Andrä et al.	Digital rock physics benchmarks - Part I:Imaging and segmentation	2012	Geology	Three approaches (1 - threshold and watershed; 2 - OTSU and threshold; 3 - Smoothness filter and threshold)	No	Computed tomography	Region Growing
El-Zehiry et al.	A SPLICE-GUIDED DATA DRIVEN INTERACTIVE EDITING	2013	General objects	Graph and energy minimization framework	previous segmentation and user entry points	Computed tomography and Magnetic Resonance Imaging	Graph-Based

Table 1 (continued)

Autor(s)	Title	Year	Area	Method	A priori knowledge	Type of image	Category
Yuankai Qi et al.	3D Segmentation of the Lung Based on the Neighbor Information and Curvature	2013	Human Healthy	Minimization framework based on level set functions	Neighbor data and grayscale informations	Computed tomography	Level Set
Yu Bing-Chang et al.	3D Segmentation of Maxilla in Cone-beam Computed Tomography Imaging Using Base Invariant Wavelet Active Shape Model on Customized Two-manifold Topology	2013	Human Healthy	Shape models and evolution	Training and landmark input	Cone-beam Computed Tomography	Model Based
Chaves et al.	Integrating discretization and association rule-based classification for Alzheimer's disease diagnosis	2013	Human Healthy	Threshold based on histogram and Association Rule mining	Training	Single Photon Emission Computed Tomography and Positron Emission Tomography	Miscellaneous
Pazokifard et al.	3-D Segmentation of Human Sternum in Lung MDCT Images	2013	Human Healthy	Graph-cut and refinement by active contour	Sternum anatomy	multi detector computed tomography	Graph-Based
Grosgeorge et al.	Esophagus Segmentation from 3D CT Data Using Skeleton Prior-Based Graph Cut	2013	Human Healthy	Graph-cut and skeleton model	skeleton model construction and landmarks for registration	Computed tomography	Graph-Based

Table 1 (continued)

Autor(s)	Title	Year	Area	Method	A priori knowledge	Type of image	Category
Ontiverosa et al.	Computed Tomography 3D edge detection comparative for metrology applications	2013	Metrology	Various methods	Variable based on the analyzed method	Computed tomography	Several algorithms
C.Shi et al.	Greedy Algorithm Based Deformable Simplex Meshes Using Gradient Vector Flow as External Energy	2014	Human Healthy and General	Deformable models	No	Computed tomography	Model Based
Paulano et al.	3D segmentation and labeling of fractured bone from CT images	2014	Human Healthy	Region growing	Initial seeds	Computed tomography	Region Growing
Antony et al.	Automated 3D Segmentation of Multiple Surfaces with a Shared Hole: Segmentation of the Neural Canal Opening in SD-OCT Volumes	2014	Human Healthy	graph-based approach that incorporated shape priors	shape priors	spectral-domain optical coherence tomography	Graph-Based
Werz et al.	Particle tracking during Ostwald ripening using time-resolved laboratory X-ray microtomography	2014	Material analysis	Watershed and distance map	No	Microtomography	Region Growing
Santos et al.	Automatic detection of small lung nodules in 3D CT data using Gaussian mixture models, Tsallis entropy and SVM	2014	Human Healthy	Support Vector Machine and threshold	Training	Computed tomography	Neural Network
Czabaj et al.	Numerical reconstruction of graphite/epoxy composite microstructure based on submicron resolution X-ray computed tomography	2014	Human Healthy	Template-matching and tracking algorithms	Templates selection	Microtomography	Miscellaneous

Table 1 (continued)

Autor(s)	Title	Year	Area	Method	A priori knowledge	Type of image	Category
Rudyanto et al.	Comparing algorithms for automated vessel segmentation in computed tomography scans of the lung: the VESSEL12 study	2014	Human Healthy	Comparison of Vessel segmentation algorithms	Variable based on the selected method	Computed tomography	Several algorithms
Ziyue Xu et al.	Efficient Ribcage Segmentation from CT Scans Using Shape Features	2014	Human Healthy	fuzzy connectedness	no	Computed tomography	Miscellaneous
Pawel Badura et al.	Soft computing approach to 3D lung nodule segmentation in CT	2014	Human Healthy	Thresholding using OTSU and diffuse connectivity	Seed information	Computed tomography	Region Growing
Jodoin et al.	Left-Ventricle Segmentation of SPECT Images of Rats	2015	Animal Healthy	Change of space and graph cut	Insertion of a T shaped target	Single Photon Emission Computed Tomography (SPECT)	Graph-Based
Hong Song et al.	Kidney segmentation in CT sequences using SKFCM and improved GrowCut algorithm	2015	Human Healthy	fuzzy C-means with spatial information and improved GrowCut	No	Computed tomography	Miscellaneous
Vasquez et al.	Automatic Framework for Extraction and Characterization of Wetting Front Propagation Using Tomographic Image Sequences of Water Infiltrated Soils	2015	Geology	Stochastic Region Merging and Multi-Otsu thresholding	No	Computed tomography	Graph-Based
Akkus et al.	Semi-automated segmentation of preoperative low-grade gliomas in magnetic resonance imaging	2015	Human Healthy	Image registration, probability map and geodesic active contours	Brain anatomical atlas and ROI	Magnetic resonance imaging	Model Based

Table 1 (continued)

Autor(s)	Title	Year	Area	Method	A priori knowledge	Type of image	Category
Fabijańska et al.	3D Segmentation of the Cerebrospinal Fluid from CT Brain Scans using Local Histogram Similarity Map	2015	Human Healthy	Similarity between histograms measured by Bhattacharyya distance and Threshold using OTSU	Insertion of an elliptical seed	Computed tomography	Miscellaneous
Hadjiiski et al.	Treatment response assessment for bladder cancer on CT based on computerized volume analysis, WHO and RECIST Criteria	2015	Human Healthy	3D and 2D level set	Approximate bounding box for the lesion of interest	Computed tomography	Level Set
Mezlini et al.	High resolution volume quantification of the knee joint space based on a semi-automatic segmentation of computed tomography images	2015	Human Healthy	Morphological operators, Threshold and active contour	Selection of a volume of interest	Computed tomography	Model Based
Biesdorf et al.	3D SEGMENTATION OF VESSELS BY INCREMENTAL IMPLICIT POLYNOMIAL FITTING AND CONVEX OPTIMIZATION	2015	Human Healthy	Polynomial fitting, Convex optimization and tracking along the central line	Initial points in the central line for the first slice	Computed tomography Angiography	Miscellaneous
X. Wan et al.	Visualization of Multiple Anatomical Structures with Explicit Isosurface Manipulation	2015	Human Healthy	Isosurface manipulation	Seeds for the segmentation process	Computed Tomography Angiography and Computed Tomography	Miscellaneous

Table 1 (continued)

Autor(s)	Title	Year	Area	Method	A priori knowledge	Type of image	Category
Kitrungrotsakul et al.	Supervoxels based Graph Cut for Medical Organ Segmentation	2015	Human Healthy	Graph cut and super-voxel (clustering)	No	Computed tomography	Graph-Based
Hemmat et al.	Semi-automatic 3D segmentation of carotid lumen in contrast-enhanced computed tomography angiography images	2015	Human Healthy	Level set function	Selection of region of interest and seed points	Computed tomography Angiography	Level set
Difei Lu et al.	Iterative mesh transformation for 3D segmentation of livers with cancers in CT images	2015	Human Healthy	Mesh transformation and contour optimization	Manually defined landmarks	Computed tomography	Model Based
Gangsei et al.	Automatic segmentation of Computed Tomography (CT) images of domestic pig skeleton using a 3D expansion of Dijkstra's algorithm	2016	Animal Healthy	Threshold and Dijkstra algorithm expansion	Knowledge about orientation, dimension of the bones and know reference points	Computed tomography	Graph-Based
Pawel Badura et al.	Calibrating level set approach by granular computing in computed tomography abdominal organs segmentation	2016	Human Healthy	Level set and Fuzzy	organ model or seed point	Computed tomography	Level set
Javaid et al.	A novel approach to CAD system for the detection of lung nodules in CT images	2016	Human Healthy	Thresholding, K-means and Support Vector Machine	Training	Computed tomography	Threshold

Table 1 (continued)

Autor(s)	Title	Year	Area	Method	A priori knowledge	Type of image	Category
K. Y. Chang et al.	VESSEL SEGMENTATION BASED ON BONE-TO-BONE ELIMINATION IN BRAIN CT ANGIOGRAPHY	2016	Human Healthy	Thresholding and morphological operations	No	Computed Tomography Angiography and Computed Tomography	Threshold
Karvonen et al.	3D Reconstruction of Cochlea Using Optical Coherence Tomography	2016	Animal Healthy	Superpixels and diffusion maps	no	Optical Coherence Tomography	Miscellaneous
Weidong Zhang et al.	Fully Automatic Colon Segmentation in Computed Tomography Colonography	2016	Human Healthy	Fuzzy connectedness and cascade of Adaboost classifiers	pre-trained colon atlas probability map	computed tomography colonography	Miscellaneous
Valente et al.	Automatic 3D pulmonary nodule detection in CT images: A survey	2016	Human Healthy	Survey with various methods	Dependent on the method being analyzed	Computed tomography	Several algorithms
Gonçalves et al.	Hessian based approaches for 3D lung nodule segmentation	2016	Human Healthy	Hessian Matrix and threshold	Initial localization of an initial nodule	Computed tomography	Miscellaneous
Ye Zhan Zeng et al.	Liver vessel segmentation based on extreme learning machine	2016	Human Healthy	Extreme machine learning	Training	Computed tomography	Neural Network
Yeonggul Jang et al.	Geodesic Distance Algorithm for Extracting the Ascending Aorta from 3D CT Images	2016	Human Healthy	Hough transform and geodesic distance	No	Coronary Computed Tomography Angiography	Miscellaneous

Table 1 (continued)

Autor(s)	Title	Year	Area	Method	A priori knowledge	Type of image	Category
Migliori et al.	A framework for computational fluid dynamic analyses of patient-specific stented coronary arteries from optical coherence tomography images	2017	Human Healthy	Thresholding	No	Coherence Tomography images	Threshold
Jung won Cha et al.	Volumetric analysis of respiratory gated whole lung and liver CT data with motion-constrained graph cuts segmentation	2017	Human Healthy	Graph cut, a trained shape model and estimation of local motion	Training and seed selection	Computed tomography	Graph-Based
Farzaneh et al.	ATLAS BASED 3D LIVER SEGMENTATION USING ADAPTIVE THRESHOLDING AND SUPERPIXEL APPROACHES	2017	Human Healthy	Thresholding and superpixel	Structural liver information	Computed Tomography	Threshold
Farzaneh et al.	Automated Subdural Hematoma Segmentation for Traumatic Brain Injured (TBI) Patients	2017	Human Healthy	Tree bag classifier and level set	Training	Computed Tomography	Miscellaneous
Shuo Wang et al.	Central focused convolutional neural networks: Developing a data-driven model for lung nodule segmentation	2017	Human Healthy	Central Focused Convolutional Neural Networks	Training	Computed tomography	Neural Network
Gibson et al.	NiftyNet: a deep-learning platform for medical imaging	2018	Human Healthy	Deep learning	Training	Computed tomography	Neural Network
Pawel Badura	Virtual bacterium colony in 3D image segmentation	2018	Human Healthy	Bacterium Colony Segmentation	Seed points/regions and non-object mask (if provided)	Several image types	Miscellaneous

spline to approximate the segmentation. They can be fully automated or supervised, where an input seed information is required to start the segmentation. Using a voxel-merging strategy, the region growing-based methods are also found in the literature. This category of methods are generally based on a bottom-up strategy, starting from pixel-level as initial regions and analyzing the neighborhood areas searching for other regions that satisfy some similarity criterion. Combining the aforementioned methods associated with the use of prior knowledge, there are the model-based segmentation techniques (deformable or not). These methods guide the segmentation process based on a known shape and spatial localization of the voxels/regions on the volume, as well as the relationships among them. Using a different paradigm, the use of Neural Networks are also used for 3D segmentation. Neural Networks is a bio-inspired computational model where a two-step procedure composed of training and testing is used. For the training step the input layer uses the information provided by other segmentation methods aiming to learn a classifier and perform segmentation on other images. There is also a general category of segmentation methods named here as Miscellaneous, grouped according to specific concepts not included in the aforementioned categories. For this one, the type of methods included are Association Rule mining, Connected Component, Dynamic Programming, Genetic algorithms, Fuzzy Connectedness, Hessian Matrix Based, Histogram Based, Polynomial Fitting, Template-Matching, and Tensor voting. This category also includes works developed as a combination of the previously published methods in some kind of hybridization.

Threshold Methods

Threshold-based methods were one of the first and simplest segmentation techniques developed. The proposed method basically use a threshold value to turn a grayscale image into a binary output corresponding to the regions of the same. The method runs through all the image pixels and if the pixel value is above the determined threshold value, the pixel is set to the maximum value from the scale used (minimum otherwise).

Besides the scope of this paper should consider works published over 2006 to 2018, one of the first approaches using a threshold segmentation strategy, for the bi-dimensional case, was proposed by Katz [11] in 1964, and the first survey was published by the end of the 1970s by Weszka [12]. After that, many surveys and techniques related to threshold methods can be verified for the bi-dimensional case.

For the three-dimensional case, three methods specifically applied to volumetric information, and found in our literature review, are proposed.

The first is presented by Li Zhang et al. [13], where a 3D method for segmentation of the choroidal vessels and quantification of choroidal vasculature thickness and choriocapillaris-equivalent thickness of the macula, in spectral domain optical coherence tomography (SD-OCT), is proposed. The proposed method has some pre-processing steps such as a three-stage approach to change the contrast of the silhouette regions in the choroidal layer and to reduce the likelihood of incorrect segmentation due to retinal vessel silhouettes; and using a graph-based multilayer segmentation approach in the OCT volume to reduce the geometric distortion of the choroidal layer and selected the target region to use the choroidal vasculature segmentation method; The choroidal vasculature segmentation consists of two main steps: vessel detection and vessel segmentation. For the vessel detection, the choroidal vessels were modeled as 3D tube-like objects in a resampled subvolume and multi-scale Hessian matrix analysis was executed to detect the choroidal vessel voxels. For the vessel segmentation, voxel groups with relatively high vesselness values, were selected by thresholding of the vesselness map. Lastly, a thin plate spline (TPS) approach was applied to the flattened segmentation result and to envelop the upper and lower surfaces of the choroidal vasculature segmentation result. To evaluate the proposed method, a reproducibility analysis was conducted in 43 SD-OCT scans using three reproducibility indices: overlapping rate, skeletonized overlapping rate, and Dice coefficient.

The second is presented by Javaid et al. [14], where a method for detection of lung nodules in computerized tomography (CT) images is presented. The proposed process begins with the tomographic volumes pre-processed through the application of contrast enhancement filter. After that, the lung region extraction is performed from the lung CTs with the use of a thresholding method associated to a contour refinement with morphological operators. The thresholding value is directly related to the segmentation quality; therefore, this value is chosen based on the analyzed volume histogram. The next step consists on the localization and segmentation of potential nodule candidates. This stage is composed of two steps: (i) all nodule candidates are detected and segmented; (ii) a refinement is performed for nodule stucked in blood vessels and bronchioles. For the initial segmentation, the k-means method is used, assigning the voxels to three classes (background, parenchyma tissue, and nodule candidates). For the identification of nodules bind to ramifications, the morphological opening operator with a specific shape, to break the 2D connections between ramification and nodules, is employed. To remove 3D connections between them, a comparison strategy is used by the 3D connected region area for each slice, i.e., if the difference between the largest with the smaller areas is greater than a given threshold, then the structures with

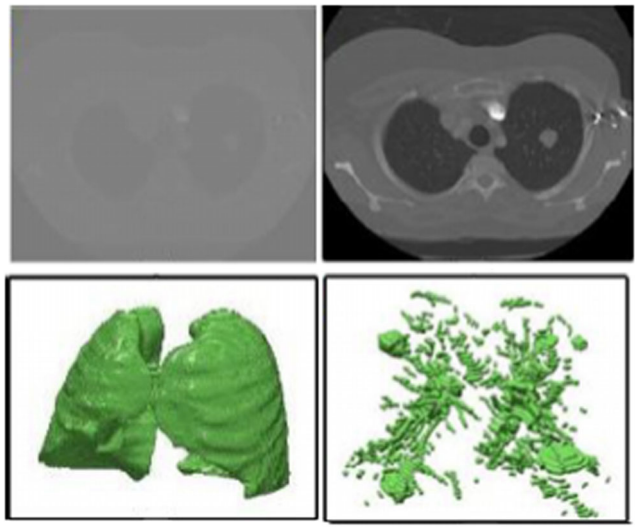

Fig. 1 Representation of the method proposed by Javaid. Extracted from [14]

smaller areas are removed. The potential nodule detection is divided into six groups and for each group features are extracted for classification and false positive removal. The classification process is realized through the support vector machine (SVM), for big nodules, and with a rule based scheme for small nodules. Figure 1 shows a representation of the proposed method. The proposed approach was applied on a set of 110 tomographic volumes from the Lung Image Database Consortium database and on the clinical images from Mayo hospital [15]. For the evaluation process, the resulting images were compared with manual segmentation performed by two specialists in terms of sensitivity, specificity, accuracy, and the number of false positive values for each analyzed case.

The third method is presented by K. Y. Chang et al. [16], where a vessel segmentation method in brain computed tomography angiography (CTA) is shown. The proposed method employs CT and CTA images using a simple tresholding technique in both images, performing after a comparison between the image pixels and removing bone structures, based on their gray levels. Then, an erosion process is applied to remove all the remaining bone boundary pixels followed by a conditional dilatation. Lastly, with the vessel regions isolated from its neighborhood, a 2D or 3D region growing algorithm can be applied to extract the vessel structure. The authors explain that several experiments were performed, showing that the method works quite well if vessels and bones are connected visually in CTA images.

The fourth method is presented by Migliori et al. [17], where a method for 3D reconstruction, applied to optical coherence tomography (OCT), is explored. The proposed 3D reconstruction method is composed of four stages: image pre-processing, lumen contour detection, stent struts detection, and alignment and orientation of detected lumen contours and stent struts with the vessel centerline. In the image pre-processing stage, the OCT frames are converted to grayscale and the line dividing the two vessel visualization modalities is used to isolate the vessel cross-section. Then, pixels belonging to the OCT visualization tools are removed by forcing their grayscale values to zero. The processed images are converted in polar coordinates aiming to express the position of each pixel through radial and angular coordinates that are centered on the OCT catheter. The catheter covers a region at the top of the image in polar coordinates and it is deleted by image global thresholding at a selected image portion. In the lumen contour detection stage, regions with higher intensity pixels are isolated, the salt-and-pepper noise is removed from each image, by applying an intensity thresholding followed by other morphological operations. The obtained binary mask is convolved over the grayscale image. In the stent struts detection stage, a fuzzy logic approach is applied, in the first sets of high-intensity pixels, to identify strut pixel and delete false positives. This procedure is possible due to the peculiar characteristic of OCT images, where stent struts appear as high reflecting elements followed by a trailing shadow. At the end of the procedure, each image is converted back to Cartesian coordinates. Lastly, is the alignment and orientation of detected components, where the detected lumen contours and stent struts are aligned with the centerline of the artery phantom.The alignment method includes the superimposition of lumen contours on the corresponding vessel centerline point and, subsequently, the orientation according to Frenet–Serret formulas, which resemble the alignment of OCT frames perpendicularly to the curve. Two point clouds are obtained from this last stage, one for the lumen contours and one for the strut centroids. The results from the proposed method were evaluated against manual segmentation by two independent expert image readers, through the computation of similarity indexes (Jaccard, Dice, Sensitivity, and specificity).

The last method is presented by Farzaneh et al. [18], where a method for segmenting CT liver images using atlas information, adaptive threshold, and superpixel is proposed. The proposed method starts by registering annotated images and creating a Bayesian probability model that accounts for location and intensity. Then, for each volume slice, an adaptive threshold is applied based on the calculated Bayesian model. Next, the anatomical information is incorporated into the approximate liver region, generated in the previous step, to create a new ROI. Lastly, the liver is segmented using the determined ROI and the superpixel generated by the Simple Linear Iterative Clustering (SLIC). The experiments performed with the proposed method where evaluated and compared with the authors' previous

approach, and with a version without the superpixel generation, in terms of Dice, Jaccard, sensitivity, specificity similarity values.

Graph-Based Approaches

Methods based on graph theory have a structure that can be represented as a graph, where the graph cut method is performed searching, on this structure, for the minimum cut on the graph providing the segmentation result. The seminal work using graph for segmentation process was the study presented by Boykov et. al in 1998 [19]. On the proposed work, the author used the graph theory to find the global minimum of energy function through a minimum multi-way cut on a graph using a greedy method for computing a multi-way cut. After that, a variety of methods emerged applied for bi-dimensional cases [20]. Due to the practical representation and the wide variety of methods for segmentation, the application of graph techniques for volumetric data was inevitable. On the delimited range of search, a total of 18 studies were found that explain how the graph theory was used for 3D segmentation applied to CT images.

In [21], a graph-based segmentation technique based on the live-wire 2D method is presented with two significant changes: the cost map based on wavelet and the clusterization through Fuzzy C-Means (FCM). These two modifications have increased the accuracy and reduced the computational cost of the proposed solution. The live-wire 2D has as base a frontier analysis and can be described on the follow steps: Image cost map calculation, which reflects the pixel edge property; Image representation by a graph wherein each vertex corresponds to a pixel associated with one element in the cost map and the edges link the vertex with each one of its eight neighbors; Optimal paths localization on the graph; and the desired frontier selection based on a seed point, a free point and an interactive segmentation method. The segmentation process ends when a closed contour is found, which extends the contour to the rest of the volume for the 3D case. The 3D approach uses the same live-wire 2D notion including the use of morphological operators, hole filling, clustering through FCM, and the next slice contour detection. The process is completed when there is no further appearance to be processed on the segmented structures. The proposed method was tested on CT and MRI images of the lungs and knees joint, being evaluated based on the resistance-to-noise approach.

In [22], Jiamin Liu et al. present 3D segmentation method of the bones joints in MIR and CT. The proposed method can be summarized in the following steps: Segmentation of the bone in scene C1 corresponding to Position 1; Selection of a Volume of interest (VOI) corresponding to the bone in scenes C1 and C2; Registration of the VOI scenes C1 and C2; and matching the segmentation corresponding to the VOI scene of C1 with the VOI scene of C2. For the segmentation of the bone in scene 1 corresponding to Position 1, the live wire method is employed. This method uses an input from the user, selection of a boundary point, to display in real time an optimum path from the initial point to any current position of the cursor. In particular, if the cursor is positioned near the boundary, the live wire snaps onto the boundary. In live wire, pixel vertices are considered to be the nodes of a directed graph, and each pixel edge is considered to be oriented and represents two directed arcs. The output of this first step is a binary scene C1 representing a segmentation of B. For the VOI selection, a rectangular box is determined, which the faces are parallel to the coordinate planes of the scene coordinate system and which encloses B with a gap of a few 5–10 voxels all around. A VOI of the same size is determined for the scene C2, with a manual adjust. For the registration of the VOI scenes C1 and C2, different methods of registration while dealing with MRI and CT scenes. For MRI the scenes are registered by maximizing the mutual information between C1 and C2. For CT scenes, a method based on landmarks is employed. Lastly, for matching the segmentation corresponding to the VOI scene of C1 with the VOI scene of C2, the result obtained in the last step is used as model to search in C2 a position and orientation of this model that best matches the boundary and the intensity pattern and, subsequently, obtain the final segmentation of B in C2. The proposed method was tested in CT and MRI images and the performance was evaluated in terms of qualitative and quantitative analysis. Qualitative analysis via segmentation results display and quantitative analysis via calculation of measures such as precision, accuracy, and efficiency.

Another graph-based approach, proposed by Aslan et al. [23], is a framework for 3D segmentation of trabecular and cortical bones on CT images. This framework and its posterior evolution [24], which has the adding of the matched filter for the automatic localization of the vertebral region, use the application of two methods separately: graph cut and volume local growing, to segment the trabecular and cortical bones. On the graph cut method, each vertex on the graph represents a voxel and the weight of each edge is defined based on the segment regional properties, integrating the linear combination of Gaussian with the Markov Gibbs Random Fields (MGRF). The segmentation process, basically, consist on finding the min cut graph, which is computed by the *s-t Min-Cut/Max-flow* algorithm. The volume local growing uses a global criterion to segment the image components. The criterion used has as base the mean intensity and the standard deviation on the 26-neighborhood. The proposed framework results were presented with an accuracy measurement and validation

on 16 sets of computed tomography images with theirs respective ground truth. Also, the European spine phantom, which is a pattern accepted for the quality control on bones densitometry, was taken in consideration.

The study presented by Kongkuo Lu et al. [25], also uses a graph-based technique. In his work, two approaches for segmentation of lymph nodes, from chest central part on CT images, are proposed. On both approaches, the user gives an initial information on a reference slice and, starting from this initialization, the methods perform the segmentation. The two proposed approaches, single-section live wire and single-click live wire, have as base the 2D live-wire algorithm, which is an edge detector method that defines the segmentation problem as an optimal search in graph by means of active contour analysis. Based on this algorithm, the two approaches for 3D segmentation were proposed: On the single-section live wire, the base algorithm is used to define the desired region contour on the reference slice. This contour is then projected for the remaining slices and the initial seeds are defined based on the pixels that compose the contour region. A set of adjusted seeds is then defined based on the pixels within the marked region and the live wire iterates until converges or reach the stop condition. On the single-click live wire, the steps are similar to the previously presented approach, changing only on the region of interest (ROI) definition. This modification is so that on the single-click, the user needs only to select a starting pixel inside of the ROI and the limit region will be defined automatically. The starting seeds are defined by the rays propagation in several directions starting from the informed pixel. The pixels with higher gradient of magnitude, along their respective ray, will be the seeds and the remaining processing steps are the same to the first approach. The experiments with the proposed methods were performed on a chest tomographies database, measuring the proposed approaches accuracy, reproducibility, processing time and success rate.

The approach proposed by X. Liu et al. [26] demonstrates a method for segmentation of iceballs on CT and MRI images. The proposed approach uses graph cuts adding a prior knowledge about the objects shape, so that each iceball segmentation is initialized with the modeled shape tendency. This tendency comes from experimental derived parameters and provides the iceball separation from the surrounding anatomical structures even with similar intensity values. The prior shape modeling is derived directly from the iceball growing model, generating a series of prior shape mask images for each specific point of the cryoablation procedure. The masks are calculated through an hyperbolic sine-shaped function and are embedded to the graph cut algorithm through regional terms. The graph cut algorithm uses the max-flow/min-cut theory applying the algorithm proposed by Boykov and Kolmogory [27] to find the max flow on the graph, which generates the min cut graph. The proposed method validation occurred through experiments on eight specific points of the cryoablation procedure on two cases, one on real-time MRI-guided and the other on monitored kidney tumor ablations. The results were compared with manual segmentations using the Dice Similarity Coefficient, which is an overlap measure.

In [28], Reinhard Beichela et al. propose a method to segment the liver in Computed Tomography images. The presented approach is composed mainly of two stages: initial graph cuts based segmentation and interactive segmentation refinement. For the first stage, a initial segmentation is generated using the graph cut algorithm. The cost function employed refers to the cost of assigning a voxel to a label based on its gray-value similarity to object seed regions. For this purpose, user defined seed regions are utilized. After obtaining the initial segmentation, a volume based segmentation refinement, composed of two steps, is applied. In the first step, a chunk-based refinement is performed. The volume chunks are generated by utilizing a distance transformation, a watershed segmentation and the boundaries previously obtained. The process of adding and remove chunks is performed by the user. The second refinement step, is based on the conversion of the selected chunks to a set of deformable mesh model which enables surface-based segmentation refinement. The surface-based segmentation refinement is an iterative process, user performed, composed of three steps: surface inspection, error marking and error correction. The proposed method was tested in 20 CT images and, for performance assessment, surface- and volume-based measures were used.

Also proposed by Reinhard Beichela et al. [29] is a method for 3D segmentation of lymph nodes in CT images. The method is composed of two stages: In the first stage, initially, a pre-processing step is performed by truncating the Hounsfield units between –100 and 150 (lymph nodes approximately CT densities). Then, the user identifies the lymph node by specifying the lymph node approximate center and a directed spherical graph is constructed, so that the local region around the lymph node is transformed into a graph-based representation. This transforms the segmentation problem in an optimization (graph search) problem, which is solved by using a maximum flow algorithm. In the second stage, the following developed iterative algorithm, consisting of four major steps, is applied: Extraction of gray-value information around the user selected boundary point; utilizing a breadth-first-search on the mesh structure, similar neighboring columns are identified and added to the region set; All the node costs of the user selected columns in the region set are updated; and lastly, a new segmentation is calculated based on the modified node costs. The proposed method was tested

in 111 lymph nodes from 35 volumetric CT datasets. For performance assessment, surface- and volume-based measures were used, such as the Dice coefficient.

Next, a method for segmentation of fluids associated with retina abnormalities on Optical Coherence Tomography (OCT) images is presented by X. Chen et al. [30]. The proposed method consists of two main parts: initialization and segmentation. The initialization is composed of some pre-processing step application on the OCT image. Initially, the superior and inferior retina surfaces are determined using an 11-surface segmentation algorithm. After, a method of surface fitting, on the inferior layer, is applied and an analysis of texture properties and layer thickness is performed individually in order to find symptomatic exudate-associated derangement (SEAD) footprints. Lastly, the retinal images flattening according to thin-plate spline identified occurs. After the pre-processing step, a voxel classification is performed during the initialization step. On the voxel classification, an initial segmentation of the SEAD areas, filled with fluids, is generated through the application of a supervised voxel classification approach trained with the previously segmented superior and inferior surface voxels. This process assigns to each voxel, between the retina surfaces, a probability ranged from 0 to 1 that the voxel is inside a SEAD region. At the end of the initialization process, the probability of belonging to a SEAD region is normalized. This normalized probability map is used to restrict the graph-based segmentation process. On the segmentation part, two methods were combined, graph search and graph cut, to segment the SEAD areas, formulating the segmentation problem as an energy function minimization problem. The energy functional built has as base the cost associated with the segmentation of all surfaces, sum to the cost associated with the segmented regions and added to the cost associated with the restrictions between surfaces and regions. The surface cost function uses the graph search method, the cost function of the regions comes from the graph cut method and the restriction cost is linked to the voxels positioning related to the two defined surfaces. On this step, the initialization previously executed is integrated to the framework through the use of the probability values, where voxels with high probability were used as font seeds and voxels with low probability were used as sink seeds. Based on those information, a graph is built, which can be solved with a min-cut/max-flow algorithm, generating than the final segmentation result. A general overview of the proposed method can be visualized in Fig. 2. The proposed method was evaluated in terms of accuracy, measured through the true positive volume fraction (TPVF), false positive volume fraction (FPVF), and relative volume difference ratio. Also, a correlation statistic analysis using linear regression and Bland-Altman plots was performed,

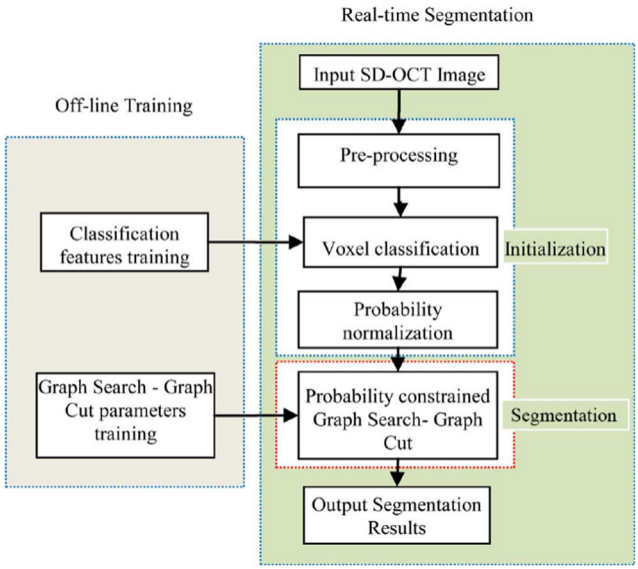

Fig. 2 Flow from the method proposed by X. Chen. Extracted from [30]

evaluating the relationship and agreement between the manual and automatic segmentation.

In [31], Pazokifard et al. present an automatic 3D segmentation algorithm to segment the human sternum in multi-detector computed tomography (MDCT) images. The proposed algorithm is divided in four steps: bone structure extraction in the lung MDCT dataset; Sternum segmentation and isolation; Segmentation refinement; and costal notches localization. To perform the bone structure extraction, first, the MDCT images are converted to a conventional image format. Then, extraneous pixels are removed with a threshold technique. Lastly, the authors employ a graph cut algorithm to remove the lungs and extract high-contrast bone structure from the dataset. For the sternum segmentation and isolation, the 3D result of bone segmentation goes through a four-step procedure that includes ignoring the half-back of the 3D bone segmentation result; finding N number of bone cross sections in mid-coronal plane; tracing all the N objects forward and removing them at each step; and applying size constraint to stop the tracing procedure for each N objects. With the sternum isolated, a refinement process is applied to remove undesired parts from the sternum, using a 2D active contour algorithm. Lastly, to determine the costal notches localization, the sternum mask is employed and the authors manually mark and determine seven costal notches in the z-direction, which are used to determine the costal notches location. The proposed method was tested in 16 patient datasets and the proposed algorithm performance was evaluated using Dice coefficient similarity, Sensitivity, Specificity, and the rates of false negative and false positive.

In [32], Grosgeorge et al. proposed a method to 3D segment the esophagus in thoracic CT scans using a

skeleton-shape model to guide the segmentation. The method has basically two main steps: 3D segmentation by graph cut and 2D propagation. In the first step, the skeleton model is constructed based on a principal component analysis (PCA). Then, this model is used to guide the 3D graph cut to segment the esophagus. In this process, the 3D segmentation overestimate from a certain slice, taking aorta into esophagus segmentation. This slice is used as breaking slice to stop the 3D graph cut and perform the 2D segmentation (2D propagation) by graph cut with a skeleton prior for the remaining slices. The proposed algorithm evaluation was performed in six patients' CTs, comparing the obtained results to manual ground truth through the Dice metric.

Different from the aforementioned graph-based approaches is the method presented by El-Zehiry et al. [33], where the obtained results, for segmentation on CT and MRI images, were submitted to an edition process. His proposal of an edition tool, has as objective to correct the segmentation results using both 2D and 3D data through the integration of all available data in one energy minimization framework. The algorithm needs a simple input, a splice 2D, generating 3D updates from the segmented volume. The edition using splice is formulated as an energy minimization problem where a graph-based approach is used for the energy optimization. Each voxel is associated with a binary variable that represents the voxel label. Each binary variable has one correspondent vertex on the graph and each existent edge is used to link neighbor vertexes, where each edge weight reflects in the energy function terms. This function has two concurrent terms: the first term aims the smoothness guided by the existent data and the second term represents the pre-segmentation. The initial seeds are provided based on an interaction via splice, which uses a set of user-inputted points to add the seed to the set of background or foreground seeds. To evaluate the proposed approach, a quantitative analysis based on a dataset of 30 liver MRI images was performed, comparing the accuracy of the edited segmentations with the segmentations performed automatically. The error measurement used was the mean point-to-surface with 2000 points.

In [34], Antony et al. present a graph-based approach for segmenting multiple surfaces with a shared hole, aiming the segmentation of the neural canal opening (NCO) in spectral-domain optical coherence tomography (SD-OCT) Volumes. In the iterative approach proposed, the original formulation of the graph-theoretic approach is used to segment the junction of the inner and outer segments of the photoreceptors and the Bruch's membrane (BM) in the volumetric image. Next, the following two steps are repeated until achieving convergence of the segmented boundary B: In the first step, a projection image is created by averaging 20 pixels above and below the BM surface. Then, the estimate of the projected boundary column B of the NCO is updated by finding a minimum closure in a graph using a graph-theoretic approach that incorporated shape priors. In the second step, the corresponding optimal set of feasible surfaces that meet at the hole boundary in the volumetric image is found by solving another single minimum-closure problem in a constructed graph. The proposed method was tested using 44 optic nerve head SD-OCT scans and the results were compared against manual delineations obtained from expert, and against two other methods, in terms of unsigned difference between: the 2D segmentation in the projection image and the manual delineations, the z locations of the automated segmentation and the manual delineations, and the 3D Euclidean distance between the automated segmentation and the manual delineations.

In [35], an iterative segmentation method based on graph cuts for segmentation of the left ventricular wall, on images of single-photon emission computed tomography (SPECT) of the rat heart, is presented. The proposed method consists of three steps: the input image conversion from Euclidean space to the spherical-cylindrical (S-C) space, the search for the myocardium center surface on the 3D S-C image and the epicardial and endocardial boundaries localization. The image conversion is given through the identification of the apex and base from the left ventricle. The identification is performed by the user input with a insertion of a T-shaped target and the casting of perpendicular to the U-shaped rays. From the T target, rays are created in cylindrical and radial directions in the 3D space. Each ray is associated with a radial angle, a height value or an elevation angle. Therefore, each Euclidean voxel, within the cylindrical area, has a ray, a radial angle, and a height or an elevation angle assigned, resulting in a 3D S-C image. For the search for the myocardium center surface, on the 3D S-C image, the graph cut method was applied, where each vertex is associated with an image voxel on the S-C space and is connected with its six closest neighbors. For the epicardial and endocardial boundary localization, the previously calculated central line is used and the myocardium thickness is calculated through the mean and variance calculation for each line, thus obtaining the ventricular wall segmentation. The proposed method results were compared against manually segmentations performed by two specialists according to the left ventricle systolic and diastolic volume calculation and against other segmentation softwares.

Vasquez et al. [36] present a framework for extracting and characterizing the dynamic shape of the 3D wetting front and its propagation, based in the processing of a tomographic image sequence. The proposed framework is composed of two modules: extraction of the 3D wetting front and characterization and description of the 3D wetting front. The 3D wetting front extraction is performed initially

via a 3D extension of the stochastic region merging, where regions are sets of voxels with homogeneous properties and grow iteratively by merging smaller regions with a stochastic test to decide whether regions should be merged. A graph is employed to structure the stochastic region merging process. After this initial segmentation, the Multi-Otsu thresholding and morphological operator applications provide the wetting front detection. For the characterization and description of the 3D wetting front, the absolute curvature descriptor was used. The proposed framework performance was demonstrated in four sequences of water infiltration in dry soils, where the obtained results were compared against estimated ground truth for the water infiltration.

In [37], an approach presented by Kitrungrotsakul et al., where a segmentation method using graph cut associated with the supervoxels, used as an optimization strategy for organ segmentation on CT images, is proposed. The segmentation using graph cut consists, initially, on the representation of each volume voxel as a node, connecting each node to its neighbors. Based on this structure, a min cut is performed on the constructed graph to discriminate the background and the foreground structures. The proposed approach performs an optimization on this structure using the supervoxel idea, which consists on the voxels clustering to generate a supervoxel set, using this set as of graph nodes and performing the segmentation on this optimized structure. For the experiments and results, evaluation of 10 CT images were used. For the proposed approach, a quantitative evaluation was given through the obtained results' comparison against the segmentation performed manually by a specialist using the Dice similarity coefficient.

In [38], Gangsei et al. present a method for automatic segmentation and identification of pig bones on CT images. To perform this process, three principles were applied: segmentation by connectivity, points and lines identification (landmarks identification), and 3D expansion of Dijkstra algorithm. For the segmentation by connectivity, a threshold value was applied and the binary result was labeled. The connected objects inside the binary image were identified through the volumes or mass center ranking. To identify the landmarks, 2D projections of the 2D skeleton were used extensively. After that, a ROI definition process, based on the landmark points and the prior knowledge about the bones orientation, is performed. Inside the ROI, the volume is seen as a stack of 2D layers and, for each layer, a virtual cut is constructed in the cutting direction. Lastly, the 3D expansion of Dijkstra is used to ensure that the resulting divided surfaces minimized the total cost for separating the bones, thus obtaining the segmentation surfaces. The algorithm starts with the last layer, and after the path on one layer was defined, a region of possible paths is identified on the next layer. All the points outside these regions are set with infinity cost and this process repeats for every subsequent layers. The proposed approach was applied on 485 CT images of pigs and the results were evaluated by visual inspection.

The last analyzed work, categorized here as graph-based segmentation, is the method proposed by Jung won Cha et al. [39]. The method is a modified version of the conventional graph cuts, where the modification is performed by adding shape prior and motion information. The shape prior information is performed by adding active shape model (ASM) with signed distance functions to the graph cut energy calculation. The motion information is added by the use of motion fields from optical flow, which warp the refined mean shape from the current phase on a point by point basis to the next phase. With the obtained warped mean shape, the extended 4D segmentation is performed via graph cuts and shape refinement using PCA analysis through the respiratory phases. Summarizing, the lung and liver boundary segmentation in 4D is accomplished by using a graph cut, a trained shape model and estimation of local motion. The proposed method was tested with 4D lung and liver segmentation using the Dice similarity coefficient to validate the obtained results against expert delineated ground truths.

Level Set Methods

The level set method was first proposed by [40] to track moving interfaces and after was used in various imaging domains. The level set general principle is to represent a contour evolution through a signed function which the zero corresponds to the actual contour. Then, according to the equation evolution, it is possible to derive a similar flow for the implicit surface that, when applied to the zero level, will reflect the contour propagation. Later, some works applied this method as an optimization framework and to computer vision and medical image analysis problems. The level set proposal had several works proposed along the years with different methods and applications [41]. Some examples of its use were found in our systematic review and are analyzed hereafter.

The work presented by Jun-Wei et al. [42] is an example of level set-based segmentation. The proposed method for extracting a lung texture tree on high-resolution CT images is described by the following steps: First, an implicit active contour model guided by an energy model, called local binary fitting (LBF), is used with dynamic parameters and modeled by the image gradient information. Then, a background painting technique based on a nonlinear intensity map is used to remove the background influence during the level set function evolution. The background removal technique is based on the human vision system

theory, where there is evidence that object recognition depends not only from the object salience, but also from the salience characteristics between the object and the background. This fact indicates that intern object details can be improved through the contrast reduction between background and object. Lastly, a comparison between the proposed method with region-based model and edge-based model was performed using a lung CT image dataset, on which the proposed approach showed a greater effectiveness on the lung texture tree extraction.

An algorithm for 3D segmentation of colon tissue on CT images and its posterior use for navigation is presented by D. Chen et al. [43, 44]. The proposed method starts with the opacified liquid removal through a threshold method and with the intern colon image intensity equalization. After that, four initial seeds are put within the colon region. Then, closed contours focused on initial seed points are propagated through the desired 3D region borders with an iterative evolution from the adaptive level set functions. During each iteration, the information on each region is estimated by parameters from the probability density function. On the presented work, a Gaussian distribution for the points belonging to both classes (colon and non-colon) was used. With the segmentation results, an isosurface is generated through the marching cube algorithm and the central line, used for navigation, is extracted by a differential equation solution. The proposed algorithm was tested on a set of 22 CT colonographies with a varied number of pathologies and was evaluated measuring its accuracy by the overlap calculation between the obtained results using the proposed method and the manual segmentation performed by a specialist.

In [45, 46], Hadjiiski et al. verified the feasibility of automated segmentation of head and neck lesions on CT scans. The method studied consists of three stages: pre-processing, initial segmentation, and 3D level set segmentation. The system uses as input an approximate bounding box for the lesion of interest. In the pre-processing stage, a set of 3D techniques, such as anisotropic diffusion filter, gradient filtering and rank transform of the gradient magnitude, are applied to the original CT images, obtaining a set of smoothed images and a set of gradient images. In the initial segmentation stage, a subset of pixels that are relatively close to the center of the lesion and that belong to smooth areas are automatically selected. The preliminary lesion contour is obtained after applying a threshold and selecting the set of pixels falling within 3.0 Standard Deviations of the mean and with values greater than 400 HU. A set of 3D image-processing techniques are subsequently applied to connect nearby components and extract an initial segmentation surface. Lastly, the initial segmentation surface is propagated using a sequence of 3D and 2D level set method. The method was tested in 26 CT scans from patients with head and neck lesions and the results were evaluated based on three measures: the intra-class correlation coefficient, the average errors for the automatic percentage change estimates in pre- to post-treatment volume and area, and the average absolute (unsigned) errors for the automatic percentage change estimates in 3D and 2D. This proposed automated segmentation method was later tested for bladder cancer segmentation in CT images [47].

A totally automatic 3D segmentation algorithm on non-contrast-enhanced angiography MRI images was presented by Hutter et al. [48]. It uses prior knowledge about irregular blood flow patterns on the carotid bifurcation area to solve susceptibility problems of the vessel affected by the flow. The proposed algorithm is divided on three steps: the first step starts with the maximum intensity projection generation on the sagittal and transversal axis from the scan slices. Then, the ROIs are identified through an adaptive threshold and noise regions are removed from the stack by searching connected areas on the slices direction. The second step is the vessel tree skeleton and the bifurcation detections. This step is performed by the common carotid artery differentiation from the vertebral artery in the first caudal slice through a pre-segmentation by size and connectivity with the bifurcation. The skeleton consists of the central point localization and the bifurcation slices. The extraction procedure is performed as follows: the threshold result from previous slice (k-1) is analyzed using an ellipsoid fitting. This gives the major axis, the minor axis, the area, and the center for each vessel segment detected. Voxels on the major axis are used as seeds for the region growing algorithm in the slice k. For each slice, a function f(k) is calculated and the bifurcation slice is determined as the slice with maximal f(k) value. Lastly, a 3D evolution level set method is applied, using the pre-segmentation process as initialization, to obtain the final segmentation result. The obtained results from 12 datasets were evaluated based on the ground truth generated by specialists in terms of sensitivity, specificity, accuracy, the positive predictive value (PPV), and the Dice similarity coefficient.

Also, in [49], an automatic lung segmentation method on CT images is shown. An estimate framework called maximum a posteriori (MAP) is used, which combines previous neighbor and grayscale information to extract the lung borders. To build the previous neighbor information model, a principal component analysis (PCA) is used on a set of training images. This model is formulated in terms of level set functions and the surfaces evolve on agreement with the associated Euler-Lagrange equations. Finally, an algorithm to refine the borders roughly generated by the MAP is used, which consist of two steps: the first step is the automatic detection and the rough lung hilo region adaptation. The second step is the rough adaptation

refinement based on the combination of curvature and probability information. The experiments with the proposed method were conducted using real lung CT images collected from a hospital.

The work proposed by Hemmat et al. [50] present a method for carotid artery lumen segmentation on contrast-enhanced computed tomography angiography (CTA) images. Initially, a ROI selection is performed, to avoid unnecessary computations, and a mean shift algorithm is used to increase the lumen region intensity homogeneity along the vessel path without any damage to edges of structures. After the mean shift, objects whose area are longer or smaller than a specific parameter are removed with morphological operators and holes are filled. Then, with three informed seed points, the center lines are extracted by a 3D Hessian-based fast-marching shortest path algorithm. Lastly, the center lines associated with a 3D level set function method are used to perform the carotid artery lumen segmentation. The proposed method validation was performed through the method application on 14 CTA volumes and its subsequent obtained result comparison with a ground truth (GT) generated by specialists. The comparison with a GT occurred with the following metrics: number of voxels, volume overlap (Jaccard and Percentage match) and agreement level between the GT and the result (Dice similarity coefficient).

Pawel Badura et al. [51] present a hybrid methodology that combines granular computing with a level set approach for image segmentation. Information granulation establishes the base for the 3D segmentation scheme employing the hybrid level set segmentation (HLS) algorithm. The follow steps are performed by the algorithm: First, the CT image data are subjected to information granulation in order to define the organ- and patient-specific granule. Then, with the granule information influence, the image fuzzification transforms the original HU intensities and enhances the organ expected intensity range. Finally, a HLS segmentation is performed over the fuzzified 3D image yielding a binary volume as a segmentation result. The proposed method has validated using 3Dircadb1 database [52], in terms of sensitivity and dice index, and compared against state-of-the-art abdominal organ segmentation methods.

Model Based

Model-based techniques are defined as "the assignment of labels to pixels or voxels by matching the a priori known object model to the image data" [53]. These types of methods try to use not only local features but also their global geometry and semantic characteristics. The next sections analyze some model-based methods with their specific features and examples.

Markov Random Fields

In 1984, the application of Markov Random Fields (MRF) was suggested to image processing (image analysis, denoising, and segmentation) [54]. The MRF is a stochastic process that includes prior and posterior distribution on the original image. For image segmentation, the MRF is used to find a labeling scheme which has maximum probability for a given set of features. In the present research, some works that use the MRF to segment tomographic image were found. Some of them are:

The work of Huang et al. [55], which presents a framework for medical image segmentation on MRI images. This hybrid framework combines 3D MRF, for the region-based labeling restriction modeling, with a deformable model for the shape-based restrictions. On the 3D MRF, each volume voxel is an observable node which is connected with hidden node representing the voxel region label. Each hidden node is also connected with six or more neighbor hidden nodes. Therefore, the segmentation can be seen as problem of MRF solution estimation using a compatibility function, between the hidden nodes, and an expectation maximization (EM) function. To integrate the deformable model part, each region label is harnessed to the 3D object surface using a graphical model theory to strictly join the two approaches. Instead of conditioning the image directly to the deformable model, the conditioning is assumed indirectly through the region labeling restriction. Based on this way of coupling between the two models, a belief propagation(BP) function is employed on the MRF part and the finite-element method (FEM) is used to infer on the deformable model part, smoothing the frontiers roughly estimated with the MRF and introducing a prior shape on the hybrid model proposed. The tests performed with the hybrid framework were, initially, on synthetic images with known objects and later on MRI medical images from a head with the skull partially removed aiming to expose the brain. The evaluation was performed qualitatively based on expert opinions.

In [56], Juslin et al. proposed a method to extract heart volume from cardiac positron emission tomography (PET) images. The method is composed of two stages: Initial segmentation using Markov Random Fields (MRFs) and heart volume extraction using deformable models. A priori knowledge about the heart positioning (anatomically the heart is located between the lungs) is used due to the fact that in PET image is possible only to identify the soft tissue and the lungs, based on the intensity values. Using this knowledge and employing the MRFs, the PET image is segmented to four tissue class background (BG), lungs (LU), soft tissue (ST), and region between thorax and background including the bed. In the heart volume extraction stage, the obtained segmentation result is used

to define the initialization for the deformable model-based surface extraction algorithm, DM-DSM (deformable models with dual surface minimization). Thus, the surface extraction is reformulated as an energy minimization problem. For the proposed method, quantitative evaluation was performed using Jaccard coefficient.

A 3D automatic segmentation for percutaneous implants is proposed by Müller et al. [57]. Based on images generated by a non-invasive optical coherence tomography (OCT) technique, Müller proposed a segmentation approach that uses MRF for skin surface estimation on the 3D space and a distortion refraction model, associated with the skin surface previously segmented, for the implant segmentation. For the OCT image morphometric analysis there is the requirement to perform the optical distortion correction induced by the tissue refraction index. This correction is performed using the percutaneous implants for the model-based estimation of the refraction index using the generalized Hough transformation. Several experiments were performed on the non-distorted model including a quantitative evaluation, with the root-mean-square deviation, aiming to show the proposal competitiveness against manually segmentation performed by specialists.

Bhole et al. [58] present an approach for 3D segmentation of abdominal CT images to identify the organs within this region. To do so, different models and modeling strategies are proposed to 3D segmentation based on MRF and their discriminative counterparts known as conditional random fields (CRF). In this work, the utility of features based on histograms of oriented gradients or HOG features are also evaluated. Aiming to segment five organs from the background the proposed approach starts with the volumes alignment with six manually selected landmarks. Then, a 3D lattice of MRF and CRF is built. After that, the variational message passing (VMP), for the HOG features learning, and the max-product (MP) inference, for the prediction in the models, are used to complete the segmentation process. The proposed approach experiments were performed on 22 volumes focused on segmenting abdominal organs and the quantitative evaluation was conducted based on the segmentation results accuracy against manually labeled volumes.

Deformable Models

The segmentation based on deformable models has as principle an estimated initial shape represented as a curve. Then, a sequence of shrinking/expansion operations are executed, based on the internal and external forces, aiming to minimize an associated energy function which ideally reaches its optimum when the curve perfectly fits the object boundaries [59]. The term deformable models was first introduced by Terzopoulos et al. [60] in 1988, were the deformable models were used for computer graphics applications. From the first time used to nowadays, it had many variations starting from how the forces were calculated to the form of optimization/minimization used [59]. In our systematic review we found some of the different deformable model types applied on tomographic data, mainly in the medical area. Some examples of these applications are:

The work proposed by Saragaglia et al. [61] presents an approach for airway wall volumetric quantification on multi-detector computed tomography (MDCT), exploiting a 3D segmentation based on patient-specific deformable mesh. The proposed method starts with the 3D airway lumen segmentation obtained by 2D method. This method performs a bronchial quantification through a segmentation method that combines mathematical morphology operators and energy-based contour matching applied to each volume slice independently. Based on this initial segmentation, the inner airway wall mesh model is built. With the focus of preserving topology and geometry of small bronchia, and obtain a regular mesh, a restricted Delaunay triangulation is applied with an adaptive distance criterion. The bronchial wall external surface is then segmented through deforming the inner wall mesh model conditionally to the image data and the shape restrictions. An equation is assigned for each mesh vertex allowing it to move in a force field governed by internal and external forces resulting in a deformable mesh model that allow a more precise region segmentation. The proposed approach was evaluated using synthetic and real data through a comparative study between the ground truth and the 2D/3D surface quantification technique proposed.

The approach presented by Hong Zhang et al. [62], aims to use a 3D segmentation method to reach the liver segmentation on CT images. The proposed method combines prior knowledge about intensity and shape to generate forces which are applied to a deformable model. The process begins with the volume codification into octree structure, based on data entropy, and a octree node classification, where each node is assigned into two groups inside or outside the liver. After that, the deformation gradient to the mean shape data depth is calculated, for each vertex, and if the computed value is less than a threshold, the force from shape is applied; otherwise, the force of intensity is applied. After the force calculation for each vertex, all the force field on each mesh vertex is smoothed and a free form deformation, with 27 control points, is applied based on the calculated forces, continuing the iteration until a stable status is achieved. The tests for the proposed method were performed with 10 real cases of CT data and were evaluated through a golden standard built by a radiology specialist, which performed the manual liver segmentation for all the 10 cases.

Ding et al. [63] work presents an organ segmentation algorithm in medical CT images. Thus, a 3D segmentation

algorithm based on deformable models to segment soft organs such as the spleen and the liver is proposed. The algorithm segments the input volume through the iterative deformation of a 3D mesh model to register it to extracted image features. In each iteration, the algorithm searches for a possible match between the mesh vertex and the image characteristics over long distances. The detected correspondence is refined before the deformation process to avoid flippings. For the deformation part, the Laplacian method is used due to the facility to incorporate geometric restrictions. In short, the algorithm can be summarized in five steps: Image feature extraction, feature matching search, detecting and preventing possible flippings, and mesh deformation. The proposed algorithm was tested in a dataset of eight CT images and compared against other segmentation algorithms in terms of noise resilience, accuracy, and execution time.

An aid system to find lung nodules on CT images is proposed by Cascio et al. [64]. The complete system is composed of six steps: isotropic interpolation, lung parenchyma volume identification, seed choice, detection, and ROI anatomic segmentation through the 3D mass-spring model (MSM), feature extraction for each ROI, and execution of classifier based on neural network. The isotropic interpolation is used aiming to reduce the possible errors due to the anisotropic grids representation. The lung parenchyma volume identification is performed with a 3D region growing algorithm and a morphological dilatation process. For the seed selection, a voxel subtraction between the binary results from the previous step and its posterior multiplication with the input image is performed, which generates the seed list. With the calculated seed list, the anatomical region segmentation process through the MSM is started. The deformable model, MSM, describes the object shape aiming to perform the segmentation and the anatomical object description. All the processes of initialization, internal and external energy calculation, and model representation and evolution are meticulously described by the author. After obtaining the nodule shape and volume, the feature extraction is performed for purposes of using the features on the nodule classification process. The obtained results were compared with other methods through the application on the same database, comparing in terms of efficiency and false positives. The validation process occurred using 84 scans from the LIDC dataset.

A method for object segmentation in 3D images, with initial user iteration, is presented by Delibasis et al. [65]. The proposed approach describes an algorithm for active/deformable surfaces, using an explicit scheme for the active surface model equation evolution. This model is built through a regular mesh that allows simple arithmetic operations to calculate partial derivatives. The user iteration can be performed in a number of ways, but the most important iteration is on the active surface initialization using simple shapes (e.g., cylinders), which directly affects the convergence and segmentation accuracy. For the external forces calculation, used in the equation evolution, the vector field convolution (VFC) is employed, which is generated using a k kernel containing vectors that point through the k origin. The proposed method results were presented through the method application in 3D synthetic data and anatomical object CT images. The evaluation was performed based on object delineation by expert users in terms of average positional error.

The study presented by C.Shi et al. [66] shows an approach for 3D segmentation in CT medical images. This approach combines the deformable simplex meshes (DSM), a greedy algorithm and the generalized gradient vector flow (GGVF) to perform the segmentation based on deformable models. Initially, the object surface is modeled with the DSM and, based on the geometric information, the internal energy needed for the deformation part is calculated. Then, the greedy algorithm is employed as an evolution method to guide the DSM to the object of interest. On each iteration, a cubic window is searched over a mesh vertex and, on this window, the energy is calculated for each vertex. The calculated energy is based on the internal energy, defined by the mesh geometry, and in the external energy, calculated by the GGVF application. The GGVF uses a variational equation to propagate the input image gradient vectors in homogeneous regions through an iterative optimization process. The mesh deformation is repeated until the vertex movements in one iteration are less than a specific value. The proposed approach experiments were conducted in a set of synthetic and real data and its quantitative evaluation was performed through the medial radial error application on the segmentation results according to a ground truth.

In [67], Difei Lu et al. proposed a multi-resolution mesh segmentation algorithm for 3D segmentation of liver. This algorithm, named iterative mesh transformation, deforms the mesh of a ROI by iteration between two tasks: mesh transformation and contour optimization. The mesh transformation deforms the 3D mesh based on the deformation transfer model, searching for an optimal mesh. The contour optimization searches the optimal transversal contours of the ROI by applying the dynamic programming algorithm to the intersection polylines of the 3D mesh on 2D transversal image planes. The initial constrains for mesh transformation are defined by manually defined landmarks, which are progressively updated by adding vertices calculated in the contour optimization task. The proposed iterative mesh deformation algorithm was employed in a segmentation scheme for diseased livers with cancer on CT images. This scheme is composed of seven steps: Constraint initialization,

where five manually identified liver anatomical landmarks and a set of chest wall points, detected automatically, are used, Liver mesh initialization based on the used constraints, Contour calculation, Contour optimization, Constraint updating, Mesh transformation, and the last step is the verification of the number of iterations, where the scheme returns to the contour calculation step if the number of iterations was not reached. The proposed scheme was evaluated using 40 hepatic CT cases, which were segmented manually by two radiologists. The proposed scheme performance was assessed using five evaluation criteria (OE: volumetric overlap error, RVD: relative absolute volume difference, ASD: average symmetric surface distance, RSD: root-mean-square of symmetric surface distance, and MSD: maximum symmetric surface distance) and was compared with five liver segmentation methods selected from ITK-Snap (www.itksnap.org) and Seg3D (www.sci.utah.edu/cibc-software/seg3d.html).

Active Contours

A specific type of deformable model technique is the active contours, also know as snakes. It had its first appearance in 1988 introduced by Kass et al. [68] and it was described as a method of energy minimization of spline guided by internal and external forces. This method merged many vision problems such as detection of edges, lines and subjective contours, motion tracking, and stereo matching. Originally developed for single images, this technique evolved, on the last years, for its use on tomographic volumes, entering on the scope of 3D segmentation algorithms. As an example of its use on volumetric data, some works can be refereed, for example: The work reported by H. Jiang et al. [69] shows the application of a hybrid approach that uses active contours for liver segmentation on computed tomography images. First, a global threshold application to split segments of the liver, stomach, spleen, and others, from the background, is performed. With the obtained binary result, the morphological operations of erosion, to remove small tissues, and dilatation, to keep the original liver shape, are applied. The next step is the use of the Sobel operator to identify the previous resulting image edges. Using the edge as a continuous and closed curve, for the active contour algorithm initialization, the active contour, for the liver on the current slice, is obtained. For the remaining slices, the found active contour on the neighbor slice is used for initialization, finding, for each slice, the correspondent active contour and, consequently, obtaining the liver segmentation. The experiments to test the proposed approach were performed on five sets of abdominal computed tomography and the validation occurred through the method obtained results comparison with the liver manual segmentation performed by specialist.

Other examples of works related to the active contours use associated with other methods are: the work proposed by Barbosa et al. [70] where a segmentation framework enhancement based on active contours, for CT and ultrasound images segmentation, is presented. The proposed enhancement is based on the framework presented by Duan [71], which shows the volume through an interface of explicit representation called Active Geometric Functions (AGF). The framework main concept is to model the interface as an explicit function which implies that, geometrically, one of the interface coordinates points is expressed as a function of the remaining coordinates. The proposed enhancement express the explicit functions as linear combinations of b-spline base functions and the problem of segmenting an object from the background becomes a problem of energy function minimization according to the b-spline coefficients, taking into account the volume local and global characteristics. Aiming to evaluate the proposed enhancement, some experiments were performed using real and synthetic data. Initially, the comparison against the framework proposed by Duan, in terms of accuracy (measured with the root mean square error) and execution time, were performed. Then, a comparison of the approach against a level set method in terms of DICE similarity coefficient, based on manual segmentation, was realized. Lastly, the method was tested on liver tumors segmentation on a set of computed tomography, on which a comparison against the Duon framework, based on overlap error, volume difference, mean and max distance and execution time, was performed.

The approach proposed by Urschler et al. [72] presents a framework for forensic cases analysis, on which the segmentation is an important process step. The segmentation algorithm used is an interactive foreground/background algorithm formulated as an energy minimization problem, called Geodesic Active Contour (GAC). The GAC is a model that splits the background and foreground through the definition of a hypersurface between the borders of the planes. The GAC can include priori knowledge (grayscale distribution, texture, shape restrictions) and, in the proposed approach, was used a continuous energy minimization process. Given an image, the binary representation of this image, splitting between background and foreground, is searched. This step is achieved by solving the minimization problem through the derivation and resolution of Euler-lagrange equations. The proposed approach results were obtained through the framework use on two forensic case analysis, the first with CT images and the second with MRI images.

A segmentation method for the measurement of local 3D variables in the knees articular space, on CT images with high peripheral resolution, is proposed by Mezlini et al. [73]. The approach can be divided in a sequence of

steps: the first step consists on the manual knee image reorientation due to the variety of orientations present in the images. After, a pre-processing step execution occurs, on the cross-sectional images, where a mean filter algorithm is applied to smooth the image and improve the edges. The filter application allows to find a stable quantile of grayscale levels and, consequently, split the bone segments from the soft tissue. This quantile is used as a threshold value to binarize the image. On the binary image the opening and closing operations are applied to reconnect the bone regions, fill the holes and remove soft tissue residues. The next step is the coronal image 3D segmentation, which consist on a 3D mask generation based on a 3D hysteresis threshold and the morphological closing operator to remove residual tissues and noises and extract the bone volume. The volume of interest (VOI) selection, performed manually, and the posterior labeling of different bone parts are the next steps. Lastly, the articular space extraction, using an active contour technique, and the articular space volume measurement occurs. The propose method was validated based on the reproducibility of different manual operations performed by two users on a dataset of five knee volumes and the method reliability was calculated by the root mean square coefficient variation computation.

In [74], a semi-automated segmentation method to segment low-grade gliomas from magnetic resonance imaging is presented. The method consists of five main steps: ROI creation, image registration, normal brain tissue detection, abnormal brain tissue detection, and tumor boundary detection. In the ROI creation step, for the 3D case, the user selects the tumor mass center in the axial view and, in the sagittal and coronal views, the user selects a ROI that encloses the tumor. In the image registration step, two image registration tasks are performed: intra-patient image registration and normal brain anatomical atlas to the patient's T2 image registration, in order to obtain prior normal tissue information. The normal brain tissue detection stage is based on the deformation field obtained in the second registration task followed by a mask procedure to avoid contamination of normal brain tissue with abnormal brain tissue. In the abnormal brain tissue detection stage, abnormal brain tissue within the ROI is detected by computing the posterior probability of each voxel belonging to the normal brain tissue and abnormal brain tissue. Lastly, the geodesic active contours is used to detect the tumor by shrinking the initial user defined ROI to the tumor boundary. The proposed method was tested in 30 pre-operative LGG patients and evaluated by comparing the obtained result with segmentations performed manually by three experts. From this comparison, several metrics were generated such as Dice and Jaccard index, sensitivity, specificity, positive predictive value, and negative predictive value (NPV).

Shape-Based Models

Shape-based models are generally built from a training dataset, where a mean shape and other features are extracted, based on the model built, after a matching between the model and the structure of interest on the new images [75] is searched. One of the first works using shape training models was the work proposed by Cootes et al. [76] in 1992, where, based on collection of shapes, a statistic of the points is determined producing a flexible point distribution model, which can be used during the object search into the image. One analyzed work that describes the image based on the shape is the work presented by Nain et al. [77]. In the proposed method, the authors determine a parametric model of a surface using spherical wavelet functions and learn a prior probability distribution over the wavelet coefficients to model shape variations at different scales and spatial locations in a training set. In order to exploit the multi-scale prior, a parametric surface evolution equation is derived by evolving the weights directly. As the surface evolves to fit the image data, the weights are constrained to remain within ± 3 standard deviation of their values observed in the training set. A region-based energy is used to drive the evolution of the parametric deformable surface for segmentation. The proposed algorithm was applied to segment caudate nucleus shapes from MRI scans and the Hausdorff distance was used to measure the discrepancy between the segmented shape and the ground truth. The proposed algorithm, called Mscale, was also compared to standard active shape models algorithm using the Hausdorff distance.

In [78], Moussavi et al. present a recursive algorithm called BLASTED (Boundary Localization using Adaptive Shape and Texture Discovery) to automatically extract the cells boundaries in cryon-electron tomography (cyro-ET) images. The BLASTED uses a conditional random field (CRF) framework, on which the frontiers points and the shape are inferred. The cell segmentation is performed by treating the texture frontiers as variables non-locally learned, proposing candidate points using physical features that depend on the estimated shape as well as the learned boundary texture, and classifying the candidate points using the learned texture with local and global shape context. The segmentation process begins with the slice manually labeled aiming to find all subsequent contours and set points that collectively are on the membrane cell. With this initial contour, the candidate points that can belong to the contour, on the next slice, can be predicted based on a template updated in each step. On these candidate points, an inference process that classifies which points belong to the contour is applied. The algorithm recursive part comes from the 3D inference partition of cell membrane boundary in 2D organization slice by slice. The proposed method was

compared with other segmentation algorithms and tested in a set of 20 cyro-ET images, using two customized metrics based on the used ground truth images.

Another work that describes a model using a training data is shown by Badakhshannoory et al. [79], where a 3D organ segmentation approach in CT images is proposed. The model-based algorithm used has two phases, training and test. In the training phase, using a ground truth given by a set of training data, a space which describes the organ is built. The organ space is a group of eigenvectors generated by the PCA application on the training data. In the test part, four main steps are executed: the first step is pre-processing, where the volume alignment and the starting point estimation are performed. The second step is the possible candidate generation, which occurs through the segmentation of each slice on a large number of overlapped regions. The third step is the possible candidate refinement, where the search space reduction, through the use of restrictions that incorporate the relationship between the organ regions on the volume consecutive slices, occurs. The last step is the best candidate selection, where the quality of all generated candidates is measured, in agreement with the organ space built on the training phase, and the best candidate is identified through the similarity measure between the candidate and the organ. Figure 3 shows the proposed approach flowchart. The validation and tests were performed on a liver dataset, on which the organ space was generated through 3D lung volume masks from twenty MICCAI 2007 grand challenge workshop training volumes. For the result validation, measures of sensitivity, error (mean-square), and similarity (Dice coefficient), against golden patterns, were used.

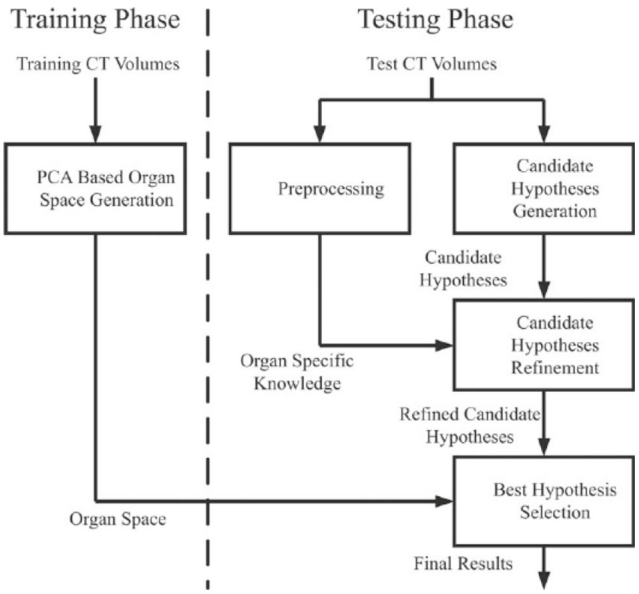

Fig. 3 Proposed method flow diagram. Extracted from [79]

The study proposed by Shaoting Zhang [80] covers some existing challenges in inference and shape refinement of image objects. Aiming to solve these challenges, Shaoting Zhang proposed a modeling framework called sparse shape composition (SSC). On this framework a set of sparse shapes is selected from a shape repository, composing them in a unique model with the purpose of inferring and refining the input shape format. The model is formulated as a learning problem using L1-norm relaxation and can be solved efficiently with an expectation-maximization (EM) method. The proposed method is independent of the data dimensionality, i.e., works for both 2D contours and 3D meshes. In the experimentation part, the method was validated on some medical applications such as 2D lung localization on X-ray images, 3D liver segmentation on low dosage CT scans, 3D segmentation of multiple brain structures of rodents on MRI images [81], and real-time tracking of left ventricle on MRI images and on tomographic reconstruction of high-resolution CT scans. In these applications, the SSC showed more robustness and accuracy when compared with some widely used approaches.

In [82], Rüegsegger et al. present a statistical shape model to precise eye modeling for treatment of intraocular tumors. To perform this modeling, initially, an atlas representing the mean shape composed only by the contour obtained through the training shapes is built. This atlas is marked with landmark points before its points are propagated for each training shape. Based on the landmark points, a statistical shape modeling can be computed using PCA. To automatically fit the model eye to a new image stack, the model is extended to use the active shape model technique, which allows an automatic correspondence of the statistical model in other image modalities. Given the built model, an iterative process search for the best fit of model profile points with patient CT images profile points through the Mahalanobis distance minimization. After a trustworthy number of matching points was found, for all profile points, the model is fitted to these profile points as close as possible. The obtained manual and automatic segmentation results, i.e., the atlas and the proposed method results, were compared in 17 CT images, measuring the Dice coefficient similarity between them.

Yu Bing-Chang et al. present a segmentation approach based on wavelet density model (WDM) applied in cone-beam computed tomography (CBCT) images from the maxilla, focusing the outer surface of anterior wall of maxilla [83]. The proposed approach can be summarized in four main steps: data acquisition and pre-processing, shape customization and landmark annotation, statistical models generation, and segmentation. In the first step, nineteen patients were scanned using CBCT; a thresholding segmentation was applied to each of these volumetric

images to obtain bone images and several algorithms were applied to obtain the bone surfaces, which were used as ground truths. In the shape customization and landmark annotation step, approaches to extract and customize a shape from the ground truth of bone surfaces, previously obtained, and generate its landmarks for statistical shape model are applied. In the statistical model generation, two statistical models are built using the training images and their corresponding training shapes. The two models built are WDM using training shapes and image feature model created by using both training shapes and training images. The last stage is the segmentation, where after the statistical models construction, the outer surface of the anterior wall of maxilla is obtained using statistical priors of the statistical models. The proposed method to perform the segmentation is the invariant wavelet active shape model (BIWASM), which based on the WDM statistical model and landmark points, performs the segmentation outer surface of the anterior wall of maxilla. The proposed method was validated using 19 sets of CBCT images and compared with other segmentation algorithms in terms of execution time, surface deviations, the closest distances, and Hausdorff distance between the ground truths and the final shapes.

Region Growing

One of the first works related to the region-growing approach was proposed by Brice et al. [84] in 1970. After that, many other region-growing methods emerged and gradually evolved this technique over the years until now [85, 86]. The region-growing method start in general with a pixel as an initial region and, basically, analyze the neighborhood searching for pixels that satisfy a similarity criterion with the region being analyzed. This process continues until it reaches an established condition (e.g., minimum number of regions or the regions stopped growing). Some analyzed works follow this principle applied to tomographic images. The first example is the approach presented by Davis et al. [87], where a method to determine a relative threshold for rough tumor volume delineation in PET images is proposed. The proposed method starts with the definition of an absolute threshold. This threshold is defined based on points belonging to the ROI and to the background. The whole process begins with a manual selection of one point inside the ROI and a second point belonging to the background. Based on these two points, an absolute threshold value is estimated. Then, a region-growing algorithm starts from the selected ROI point and a preliminary target volume based on the absolute threshold value is produced. This preliminary process may have included non-target structures; thus, to remove this structure, a third point is informed inside of a non-target structure. Two region-growing algorithms start from the maximum signal point, previously calculated, and the recently informed point. The two regions grow simultaneously and the algorithm stops before the two regions fuse into a unique region. The two-region split is performed using a Voronoi algorithm to achieve geometric separation of target and non-target volumes. Only the voxels that are inside of the target region and lie within half of the full-width at half-maximum of the PET image resolution from the absolute threshold, are included in the true max signal level final estimation. A similar process is adopted for the background average signal final estimation. Then, based on this two obtained values, the final absolute threshold, used for determinate the target volume, is calculated. The proposed method validation was performed through the use of PET images with spheres of known diameter for the automatic segmentation. Additionally, tests on images of patients with breast cancer and thymus were also performed.

In [88], a study for automatic ribcage segmentation and labeling in CT chest images is presented. The proposed system consists of five stages. The first stage is the application of a threshold, obtaining a binary image, and use of a Hessian matrix with values originated from the 1D Gaussian kernel application on the image. This process results in the detection of 1D rigid structures. These rigid structures are employed on the construction of primitives in the form of line elements on the second stage. To do so, a region-growing process is used, taking into account the rigid structure local orientation. The neighborhood around the 1D rigid voxels is investigated and other voxels that meet some requirements are added to the primitive. The primitives that meet specific constraints are called convex sets. Then, some seeds are randomly chosen from the available ridge voxels, for this region-growing process. After the convex set extraction a new seed is chosen from the remaining ridge voxels. The third stage is the primitive classification, where a classifier to differentiate the ribs from background structures, is used. This classifier maps a feature vector, extracted from the objects under investigation, to class numbers or to a vector of probabilities of belonging to a specific class. This mapping must be learned through the training data, which were previously labeled to their appropriate classes. The fourth stage is the grouping of primitives, where the objective is to group the rib primitives into specific rib centerlines and label this centerline to rib side and number. Lastly, to complete the segmentation process, a seeded-based region-growing algorithm is used, where the seeds are determinate based on the mean gray value for each centerline. The proposed method was tested on twenty CT scans and the results were evaluated qualitatively by human inspection.

In the method proposed by Monga [89], the volume images are described as a set of primitive volume patches (bowls, cylinders, cones...), aiming to optimize a criterion,

assuring its stability and including its scale characterization. This optimization occurs with a region-growing algorithm applied to an adjacency graph, which represents the primitive volumes and its adjacency relation. The proposed approach can be summarized in three steps: The first step is the data representation initialization based on Delaunay triangulation. Then, a selection of initial primitives using Delaunay spheres is performed. On the last step, the fusion of initial primitive is realized, using a minimization algorithm based on region growing. The proposed method experiments were performed on CT soil images aiming to represent the geometric porous space, which allows to join geometrical and soil properties to better characterize some application for soil science.

In [90], Bulu et al. presented a comparative study between four segmentation algorithms applied to CT medical images. The compared algorithms were two region-growing algorithms (one with initial seed points and the other without), Weibull E-SD Fields (WESDF), and an automatic multiple level threshold using OTSU. Two are fully automated (OTSU and region growing without seed points) and the other two methods (WESDF and region growing with seed points) need some user iteration level. The region growing with seed point algorithm starts its growing process from the informed seed points and, based on a connectivity criterion, extract the connected region from a 3D volume. The WESDF generates, initially, K-sized volume cubes, which are called K-voxel. Each K-voxel receives two values: expectancy and standard deviation (E-SD). Then, the Weibull filter is used to remove the image noise, making the E-SD values more precise. After the E-SD calculation, the frequency of voxels having the same E-SD is shown. The segmentation process assume that E-SD values in the same region are relatively homogeneous and they are different from those in other regions. The thresholding using OTSU, consists in the basic idea of automatically selecting a threshold value that splits objects of interest in an image from its background based on a grayscale value. The threshold value selection is based in a choice of a value that maximize the variance between histogram classes. The region growing without seed points works similar to the region growing with seed points, differentiating only in the initialization process. The region growing without seed points initializes the process with one region containing one pixel, generally in a starting slice, and the working state consists in a set of identified regions and a set of non-allocated pixels with frontiers with at least one of these regions. Then, based on a similarity criterion, the non-allocated pixels are assigned to the region with the biggest similarity value. The four method evaluation and comparison were performed in four different datasets, one for test purposes and the others with real CT images. Some measures, ranging from 1 to 4, 1 to 5, and 1 to 10, were used for the algorithm comparison (implementation, noise sensitivity, user iteration, execution time, obtained result, and general result). These measures were empirically assigned based on human observation.

Diciotti et al. [91] present other examples of region-growing-based segmentation for 3D nodule segmentation on lung CT images. The proposed method starts with the selection of a volume of interest (VOI) that has as reference a central voxel informed by the user, assuming that the lung nodule is completely included on the VOI. After, the voxel is supersampled with a trilinear interpolation to obtain an isotropic voxel and to reduce the partial volume effects. The next stage, identifies candidate markers corresponding to blob structures in the scale space. All the candidates are shown to the user for inspection and must be approved as a marker (nodular or lung structure) or object to be discarded. The region-growing algorithm use the markers on the segmentation process, seeking to avoid a possible merging between the nodule and different lung structures. The region-growing method used joins the gray level representation with the concept of geodesic distance. At the end of the segmentation process, if the obtained result is not satisfactory, it is possible to repeat the marker supervision and the segmentation process. The segmented nodule volume is extracted using a simple process of voxel counting. The proposed method was evaluated on images with small ghost nodules and on lung CT images from the Lung Image Database Consortium [92] in terms of root-mean-square error based on expert manual segmentations.

In [93], the author shows an adaptive segmentation algorithm to segment the pulmonary airway tree on lung CT images. The proposed approach consists of two steps: In the first step, the volume is roughly segmented and divided in several subvolumes through a region-growing algorithm based in a VOI. These generated segmented subvolumes are divided on three types according to their topologies. On the second step, for each subvolume type, a specific method, to find the seeds for the segmentation process, is applied. For the first type one subvolume, the seed is the geometric center of the bronchus slice on top and the initial threshold is determined based on previous works. For other types, one subvolume, the seed is the central line bifurcation on its parent type two and the initial threshold is its parent's final threshold. When the region starts to grow, the final threshold is assigned as being the initial and the final threshold is gradually increased until a leakage occurs. For the type two subvolumes, the seed is the central line of its parent type one subvolume, the initial threshold is its parent final threshold and the value adjustment is similar to the performed for the type one subvolume. For the type three subvolume, the seed is on the central line bifurcation in its parent type two, the initial threshold is its parent final threshold and the value adjustment is similar to the other subvolume

types. To evaluate quantitatively the proposed approach performance, a detection rate was defined, which take into account the number of bifurcations found by the automatic segmentation and the number of bifurcations found by the manual segmentation performed by a specialist.

In [94], De Nuzio et al. propose a 3D lung segmentation algorithm in computed tomography scans. The algorithm is composed of six steps: The first step is the image histogram analysis, aiming to find a threshold value for the segmentation of the respiratory apparatus; In the second step, a simple-threshold 3D region growing is applied to the CT volume, where voxels that contain a value smaller than the value found in the first step are included in the growing region. This step results in a binary mask of the respiratory system. In the next step, the external airways are extracted and removed by a wavefront simulation model, resulting in a mask containing only the lungs. In the fourth step, due to partial volume effects, the lungs may appear as a single object. If that happens, the fusion region is identified and a separation surface is inserted into the mask to correctly disjoin the lungs. Next, the simple-threshold 3D region growing is used twice in the last step mask, to grow the left and the right lung respectively. Lastly, morphological 3D closing is separately applied to both masks (left and right) for the inclusion of pleural and internal nodules, and to patch the concavities corresponding to vessels. The overall segmentation is the union of the two resulting masks. The proposed algorithm was initially developed on a set of 130 thorax CT scans from the Italung-CT database and after was tested in the ANODE09 (http://anode09.isi.uu.nl/) and to the LIDC [92] databases. The evaluation was performed by comparison against ground truths in terms of volume overlap and distance between contours. The sensitivity for nodule inclusion was also tested.

The work proposed by Bert et al. [95] presents another example of region-growing segmentation method, which has as purpose the colon wall segmentation on abdominal CT images. The proposed method used an approach of three stages employing a 3D adaptive region-growing algorithm with adjustable growing condition. The first stage is the external segmentation, which masks the air presented outside of the body surface. This stage is performed by using, initially, a threshold algorithm followed by a 3D region-growing algorithm. The seeds for this first region growing are resulted from the performed threshold process. The second stage is the lung segmentation, which masks the air inside the lung by using a 3D region-growing algorithm based on seeds belonging to the range between lowest image intensity value and the peak on the histogram. The third stage is the colon segmentation, which extracts the colon segments through the initial histogram generation on the actual image stage aiming to define the seed points for the region-growing process. If during the growing process a voxel value bigger than the superior limit was found, then a new value for the superior limit is calculated based on colon wall local values (adaptive part). The proposed method was evaluated comparing the obtained results with manual segmentation results, performed by specialists in 30 abdominal CT images, in terms of true positives, percentage of recognized colon surface, true negative, and false positives.

In [96], an automatic 3D segmenting method for liver segmentation in MRI images is presented. The proposed method try to use all the available MRI channel information to formulate a probabilistic framework. On this framework, a discriminative multi-class linear analysis is applied as a dimension reduction technique and a probabilistic map, used on the segmentation process, is generated. The proposed method can be divided on four stages:

- Preparation: on this stage the specialist knowledge is integrated to the method through a training process with the contour information of ten different types of liver shape provided by a radiologist. Based on this knowledge it is possible to categorize the MRI dataset points on liver tissues, kidney tissues and background.
- Probability map generation: by using a region-growing segmentation method it was noticed occasional heterogeneity on the intensity inside the liver between the left and right side. Based on this observations, the probability map generation was subdivided in three cases. The first case was the probability map generation for three classes (liver, kidney and background). The second case was probability map generation for two classes (liver and background) and the third case was the probability map generation for two classes (left liver side and background). These probability maps are determined through the pixel coordinate distribution histogram and the intensity distribution in the MRI datasets.
- Segmentation: the segmentation can be divided in three steps. In the first step, a region-growing algorithm is applied on lower resolution probability images. In the second step occurs the segmentation refinement through the region-growing algorithm application on the original probability images. In the last step, only the liver left side is segmented with a threshold technique in the longitudinal direction of the body.
- Refinement: due to the probability similarity from the tissues next to the liver it is difficult to avoid oversegmentation. To correct this limitation, a border refinement with Fourier descriptors is used, liver surface curvature analysis and a linear discriminant analysis.

The proposed method tests were performed on MRI images from patients between 21 to 79 with the most variate cases of liver volumetry and the validation was based on ground truths, manually generate by experts.

In [97], a 3D segmentation technique is presented for lung parenchyma detection on CT images. The proposed method consists of four main steps: the first step is the analyzed volume binarization through an adaptive threshold technique, on which an optimal threshold is selected, aiming to split voxels within the high-density trunk and chest structures from low-density voxels in the lung and the area outside the trunk. The second step is the application of a 3D connected component method, which is applied on the inverse image from the previous step, removing the background and highlighting the lung parenchyma. On the inverse image, only the lung parenchyma, trachea, bronchus, and nodules were preserved. The third step is the trachea and bronchus removal through a region-growing algorithm, on which the anatomical knowledge about the trachea is used to initialize the seed automatically. The growing and stop condition criteria are established based on a comparability criteria. Lastly, a sequence of morphological operators is used to smooth the borders and fill the holes caused by small vessels, trachea, and nodules. The proposed method was evaluated based on a set of 20 CT images from 20 patients using two performance measures (average segmentation accuracy and speed).

In [98], an approach for 3D segmentation on CT human brain is presented. The first part of the approach is the pre-processing step, which consists in the application of several filters (median, maximal, minimal, Gaussian, and edge detector) and other operations such as histogram equalization and normalization. The next step is the segmentation, which consists in the generation of 3D points, in the brain area, where each point is a seed for the segmentation process. Given a tolerance value, the maximum and minimum values are obtained by adding and subtracting from the tolerance value, respectively, the voxel value. Voxels in the neighborhood area with values between the maximum and minimum are added to the segment and its neighbors are analyzed repeating the process until is not possible to add more voxels to the segment. Then, the feature extraction is performed, using features such as edge, relative size, segment volume, average, geometric average, standard deviation, sum, sum of squares, min and maximum values, asymmetry, variance, and curtose. After the feature extraction step, a model is built based on the extracted features, using a decision tree as learning algorithm. The approach was tested in three sets of brain CT images and evaluated based on its accuracy with the false positive, true positive, and class precision values.

In [99], Andrä et al. show four benchmarks for physical rock simulation which includes image acquisition via CT, image processing, numerical experiments, and numerical resolution of filed equations. One of the steps, in the image processing part, is the segmentation, and on the presented work, this part is reported through three different segmentation approaches from three different research groups. The first approach, from the VSG research group, has as first part the removal of image artifacts such as noise, brightness non-uniformity, and phase-contrast fringes in the grain boundaries. Then, for better result in the labeling part, a three-step process was used. In the first step, the image magnitude gradient was calculated and threshold was used to identify all the boundaries, which are marked for exclusion in the next step. In the second step, the dark pixels from the porous space and the mineral bright pixels suffer an application of a threshold. All the pixels near or in the interface grain-porous were excluded from the selection. In the third step, each selected pixel is used as marker for a marked based watershed algorithm and the magnitude gradient is also used as input for the algorithm. The second approach, from the Stanford research group, is based on a three-step methodology. Initially, the input images are laterally cropped to remove edge artifacts appearing in the image corners. Then, a threshold value is chosen using the OTSU method. Another threshold value is manually used to distinguish ankerita and zircom minerals from quartz. Lastly, the relabeling occurs , removing all regions that are not connected with a volume less than 50 voxels. The third approach, from the Kongju research group, consists in the application of a smoothness filter to reduce the noise from the reconstructed image and the use of a single threshold value to differentiate mineral from the porous space. After the application of each approach, a porosity calculation was applied on each of the four datasets and the results were compiled in a single table providing a comparison of the influence of each segmentation approach on the rock samples physical properties calculation.

In [100], a multi-level approach for segmentation of different lung nodule types in CT images is presented. In this approach, initially, a binary mask generation occurs with functions related to some type of pre-defined nodules. Depending of the nodule type, this rough segmentation stage is performed following one or another path. The volume is initially binarized using a threshold value with the OTSU method, which allows a rough distinction between nodules and the surrounding regions. For cases where lung nodules were considered of low density, the segmentation is performed based on diffuse connectivity analysis. For other cases, the binary mask generation continues. The remaining steps are performed over the OTSU resulting image. The next step is a 26-connectivity analysis, where if the seed manually informed is different from the component with greater number of voxels, then the separation is complete denoting cases of vascularized or well-restricted nodules. If the connectivity analysis fails, then the nodule is some way connected with the pleura, characterizing nodules type 3 or 4, and a slice by slice separation is indispensable. This separation is performed with an 8-connected analysis for

each slice and on every success on the separation of the 2D nodule with the biggest segment, the mask generation stage is completed for the actual slice. The next two steps on the mask generation process are the separation of nodules type 3, with morphological operators, and type 4 through the lung edge reconstruction. The mask generation scheme can be summarized by the Fig. 4. After the mask generation, for each mask slice generated occurs the nodule central point identification. Also, the generation of seeds inside and outside the object is performed to make the diffuse connectivity analysis more representative. With the masks and the set of seed points, the robust segmentation stage is started based on the diffuse connectivity. The connectivity diffuse segmentation method belongs to the region-growing methods and describe the relation between the pair pixel/voxel in terms of a relevance function. Its value is based on the fuzzy affinity of the relations between pixels/voxels topologically adjacent, reunited using a graph search algorithm and this value determines if they belong to the same object. Lastly, the remaining vessels are removed using a post-processing step that consists in the application of morphological operators, distance transformation and the connectivity with a central nodule. The proposed method was evaluated, initially, using a set of 23 thoracic CT studies and for the final evaluation a total of 551 cases from the Lung Image Database Consortium were employed. Three main evaluation measures (true positive rate with 50 and 100% of consistency and the number of certainly non-nodule voxels) were defined based on a golden standard manually delineated by human observers.

In [101], a particle tracking during the coarsening process of the semisolid state of Al-5 wt.% Cu samples in microtomography images is proposed. To perform the tracking, a sequence of methods to remove noise, improve the contrast and perform segmentation is applied. Initially, to secure the watershed algorithm reliability, a sequence of adaptive filter, called Wiener filter, and a top-hat filter were applied to the volume slices. The next step, consists in the removal of spherical precipitates of the matrix phase embedded within the coarsening particles. The final step, before the watershed application, is the 3D Euclidean distance transformation application, which assigns a number to each voxel that is proportional to the voxel's distance from the matrix phase. Lastly, the watershed is applied, closing the voids in the matrix phase reconstruction. Once the gaps inside the particle boundaries were removed, an adjustment to the volume fraction of the matrix phase was performed by uniformly widening the particle boundaries. The result is a volume where each remaining voxel belongs, without ambiguities, to one particle, making possible to determinate the spatial extension of each particle and to label them with a unique number. To analyze the proposed method, the samples were continuously captured to get different microstructural evolution regimes during the Ostwald ripening process. The data obtained on the resulting images from the proposed method were compared with prior results obtained in experimental studies and with computational simulation from the Ostwald ripening process.

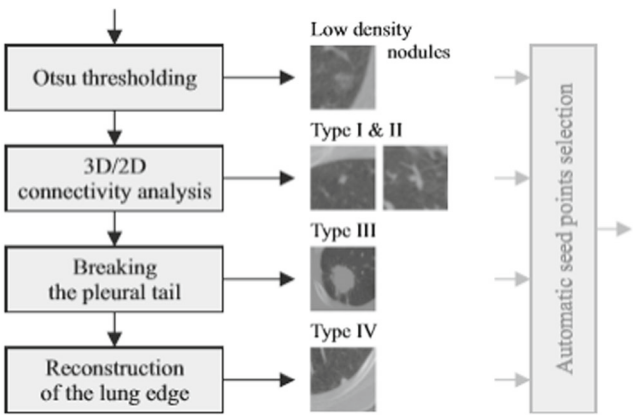

Fig. 4 Mask generation method. Extracted from [100]

In [102], the author proposed a method to perform segmentation and labeling of bone fragments in CT images. The method is based on a 2D segmentation algorithm by region growing and requires a minimum user iteration to initialize seeds in the bone fragments in the first slice that they appear. After the seed selection occurs the segmentation process on slices that the seeds were initialized such that, for each seed, the segmentation and subsequent subtraction of overlapping regions is performed, removing seeds that already belong to a segmented region. After performing the segmentation for the actual slice, all the seeds are propagated to the subsequent slice and the segmentation process previously described is repeated. To propagate the seeds, first they are inherited from the previous slice and, if the seed fails, i.e., it cannot segment a considerate bone area, its neighbors are considered seed candidates. If all the neighbors also fail, then the seed is removed. The process stops when all the seed were removed. The proposed method was tested against methods commonly used for healthy or fractured bone segmentation in CT images.

Neural Network

Neural network (NN) methods applied to image segmentation had its first appearance based on Pal et al.'s review [103] with the work proposed by Blanz et al. [104]. In this work, a trainable classifier multilayer feed-forward network was presented, with one hidden layer specifically designed to perform the image segmentation process. After that, many segmentation methods using NN were proposed over the literature [105]. On the presented systematic research, four

works were categorized as NN-based segmentation method for 3D segmentation.

The first method discussed is the approach proposed by Li et al. [106], where a sequence of algorithms for segmentation of CT and X-Ray clinical images is presented. The complete process is divided in two steps: training and segmentation. In the training step, the manually selected images are segmented using a variational level set method guided by an energy function projected to delineate the pathological features in the image. The energy function project employed the aid of an expert to model the function on agreement with the pathological features from different image regions. The next step is the features extraction through the application of a window-based method on the previous segmented images. Over the extracted features occurs the PCA application aiming to use the most relevant features on the the support vector machine (SVM) training. After the training step, the SVM is used whenever there is the need to segment an image. To evaluate the proposed method results, 2D and 3D chest CT images and X-ray images from the dental arch were used. The results were analyzed subjectively.

Another method using an NN approach is presented by Chang et al. [107]. On this approach, an algorithm for segmentation based on a model of pulse coupled neural network (PCNN), on lung CT images, is presented. The PCNN algorithm consists of tree modules: the receptive field, the modular field, and the pulse generator. The receptive field role is to receive inputs, from other neurons and external sources, by two channels, feeding channel, and linking channel. In the modular field, the inputs are modulated and the result is sent to the pulse generator, which is composed of a pulse generator and a comparator. The result is compared with a dynamic threshold to decide whether the neuron is activated or not and, in case it is activated, the pulse generator will have as output 1 and the dynamic threshold will be enlarged accordingly. This model, applied for 2D images, is expanded for 3D images with the following steps: first a 3D matrix is built with the hole volume. Then, the VOI is selected and the parameters are initialized. After, the lung volume is segmented with 3D improved version of the PCNN (the 3D I-PCNN), to obtain the binary image. As next step, the lung field is extracted from the binary image through the use of morphological erosion and contour smoothness. Lastly, the 3D binary data is multiplied with original image to obtain the lung field image, reconstructing the final volume result with a rendering algorithm. The proposed algorithm was evaluated using a dataset with five cases of CT images and the evaluation was performed through the obtained result comparison with GTs manually generated by specialists in terms of mean distance, root means square distance, and Tanimoto coefficient.

In [108] a methodology for automatic detection of small lung nodules on low contrast CT is proposed. This methodology is represented by the Fig. 5, and it can be categorized into four stages: CT image acquisition, nodule candidate segmentation, characteristic extraction, and candidate classification on classes nodule and non-nodule. For the nodules candidate segmentation, four steps were used: the first step is the lung parenchyma segmentation using threshold and region-growing algorithms. The second step consists in the previous step complementation to remove the trachea and the main bronchi through the selection, on each volume slice, of the two biggest regions. The third step segments the structures inside the lung using the Gaussian mixture models method to model the voxel intensity value distribution, from the previous step resulting image, distinguishing them into two classes: internal structures and lung parenchyma. On the last step, only structures with shape and texture with features similar to nodules are selected through the shape structure found. As the nodules are spherical structures, a Hessian matrix is used to find round structures differentiating from the others. After, on these possible candidates, a texture feature extraction is performed with an entropy calculation proposed by Shannon and Tsallis Q followed by the classification from these characteristics with the support vector machine (SVM), differentiating the nodules from other structure candidates. The proposed method validation was given by the number of true positive nodules, rate of false positives and false positives per exam, sensitivity, specificity, and accuracy values.

In [109], Ye Zhan Zeng et al. proposed an algorithm for liver vessel segmentation base on extreme machine learning (EML). First, the anisotropic filter is applied to remove noise and preserve the edges. Based on the shape and geometric structures, knowledge, and tree filters (Saito, Frangi, and offset medialness) associated with an energy of deformation filter were used to extract vessel structures. In this step, the filters Saito and Frangi were used to detect 3D structure vessel, the offset medialness was used to extract the vessel topology and the energy of deformation filter was used to improve complex structures such as bifurcations and branches. Lastly, with the previous extracted structures, three process were applied (normalization, training, and posterior classification using the EML) segmenting the liver vessels from the background voxels. The experiments with the proposed technique used six sets of abdomen CT clinical images and the result evaluation was performed with a specialist analysis through corrections on the obtained results and three calculation measures (accuracy, sensitivity, and specificity).

In [110], Shuo Wang et al. proposed a central focused convolutional neural networks (CF-CNN), to segment lung nodules from CT images. The CF-CNN model utilizes 3D and 2D views of CT imaging for lung segmentation. Thus,

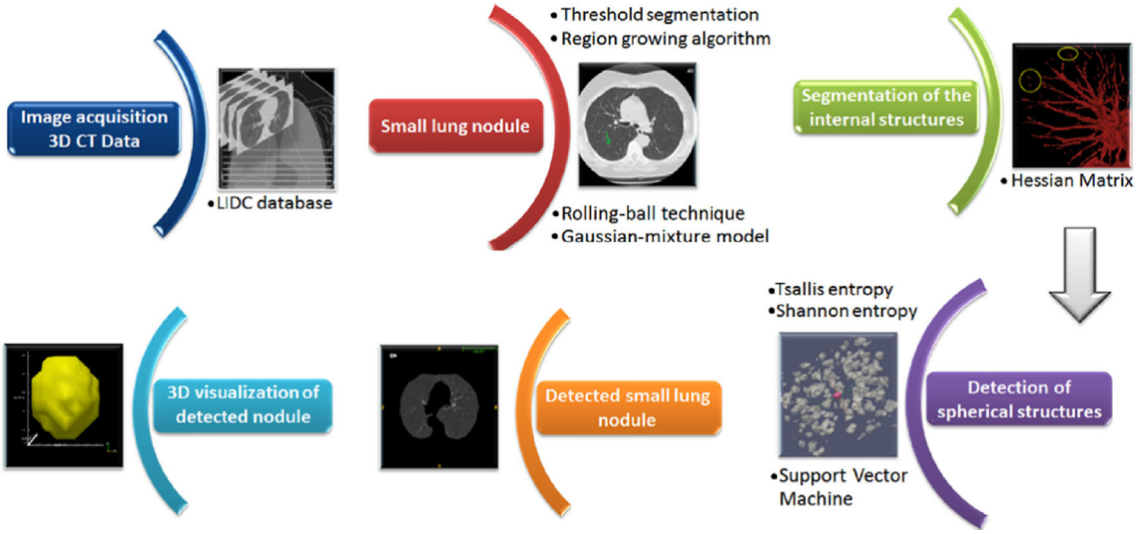

Fig. 5 Flowchart from the methodology proposed by Santos. Extracted from [108]

given one voxel in CT images, the 3D and 2D patches are extracted and used as input to the CNN model to predict if the voxel belongs to the nodule or healthy tissue classes. The author explains the model architecture, how the training samples were selected and all steps involved in the process. The test performed with the proposed approach employed two datasets: publicly available dataset from the Lung Image Database Consortium and Image Database Resource Initiative (LIDC) and the independently collected from Guangdong General Hospital (GDGH). The proposed approach was tested against several segmentation methods (Level Set, Graph Cut, U-Net, 3-D-Patch Branch, 2-D-Patch Branch, CF-CNN-MP, CF-CNN) in terms of similarity index (Dice similarity coefficient and symmetric average surface distance), sensitivity, and positive predictive value compared against a ground truth segmentation.

In the last work, Gibson et al. [111] proposed an infrastructure that provides a modular deep-learning pipeline for a range of medical imaging applications (segmentation, regression, image generation, and representation learning). This infrastructure, named NiftyNet, is built on tensorflow framework and has as main objective to address the ideosyncracies of medical imaging and to lower the barrier to adopting this technology in medical imaging applications. The author presents the infrastructure with components optimized for medical imaging applications and specific interfaces for medical image segmentation, classification, regression, image generation, and representation learning applications. Lastly, the author shows illustrative applications, such as abdominal organ segmentation, using the NiftyNet discussing over the results obtained, lessons learned, and future direction of this proposed infrastructure.

Miscellaneous

In this section, we present the works that have particular specifications and cannot be inserted into the above categories. Due to its specificity, we summarize for each work the algorithmic process employed as well as how the approach was tested and validated.

Association Rule Mining

Chaves et al. [112] proposed an aid system for early Alzheimer's case diagnoses. The proposed system consists of three steps: the first step is a mask generation and use, which is built with the use of a threshold based on an average control image histogram. Then, a discretization process is applied, consisting of an equal-width-size histogram applied to the intensity values inside the mask range, splitting them into k bins of equal width, which are used to define the intervals of the selected ROIs. These ROIs are used as input for the association rule mining (AR mining) algorithm, which, on its training phase, captures co-occurrence patterns within the control data and has as objective to use rules to classify images in two classes (control and Alzheimer's). A rule on this context is the relation between transaction item with enough support and confidence. The AR mining process employs an algorithm for finding sets of confidence and support greater than minimum support and minimum confidence defined by the user. Figure 6 summarizes the described process. The proposed system was evaluated with images from the Alzheimer Disease Neuroimaging Initiative (ADNI), using the receiver operating characteristic (ROC) curve based on the accuracy, sensitivity, and specificity values as measures.

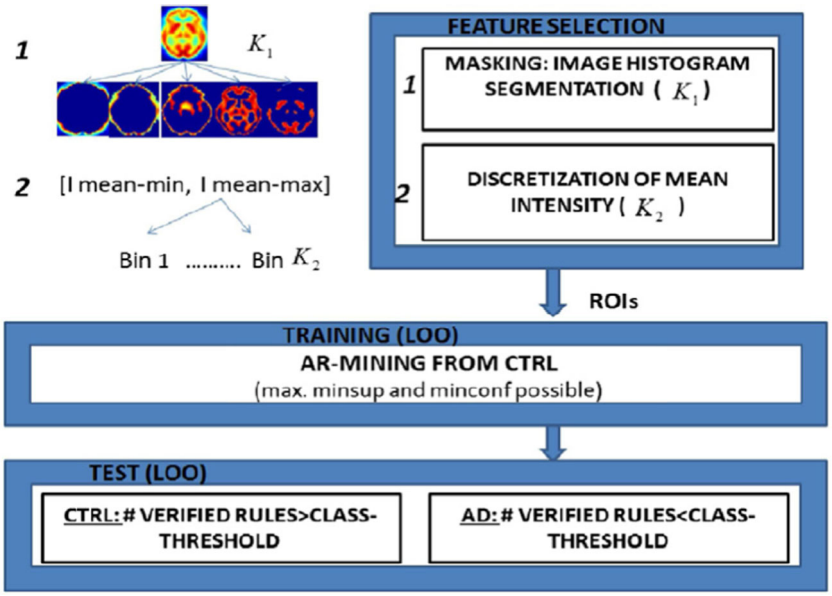

Fig. 6 Flow diagram summarizing the method proposed by Chaves. Extracted from [112]

Connected Component

Spampinato et al. [113] present a method for mandible surface segmentation and measure in CT images. The segmentation part is performed in two stages: The first stage consists on the inferior mandible-arch extraction. This step identifies a mask, which is applied to filter only the inferior dental arch and can be described by the follow steps: first step is an orientation phase, where for each volume slice, starting from the the bottom one, a bit-plane slice coding is performed. On the bit-plan slice coding, the slice is divided in several images, where each image represents the contribution of a specific bit to the total image appearance. After that, the selection of the bit plane with most significance is performed, the application of morphological operators and largest connected component identification in each slice. The mask is selected based on the connected component with the lowest ratio, calculated through the division between the connected component area and the component convex hull area. The second stage has as objective the upper mandible-arch extraction. In this stage occurs the application of the first two steps used for the lower mandible arc extraction starting from the slice where the upper mandible arch begin. Then, the connected components are computed and to be considered mandible part, they must satisfy three restrictions (position, distance, and shape). After the mandible region extraction, a surface rendering algorithm is applied for 3D reconstruction and posterior measuring between landmarks localized on the reconstructed surface. The proposed method was evaluated against measures performed by two specialists over 10 tomographic volumes: 5 from the control group and 5 from patients with facial asymmetry, in terms of mean and standard deviation.

Diffusion Maps

Karvonen et al. [114] present method for 3D segmentation of cochlear optical coherence tomography (OCT) images that is based on superpixels and diffusion maps. The proposed method has basically two steps: pre-processing and clustering. In pre-processing step, the OCT images are smoothed by a median filtering method and the superpixels are created. Then, in the clustering step, the diffusion maps are constructed using a Gaussian kernel with the Euclidean distances between superpixel intensities as the distance metric. After that, the k-means clustering method with 2 clusters (background and foreground) is applied to identify the superpixels that belong to the cochlea. Finally, the labels assigned to each pixel are used to expand the superpixels obtaining the original volume and, consequently, the volumetric binary image. The proposed method was applied in some experiments with guinea pig and mice cochleas OCT images.

Dynamic Programming

The work presented by Qian Wang et al. [115] propose a method for lung nodule segmentation in CT images. The proposed approach can be divided in two stages: In the first stage, the 2D dynamic programming model was extended to a 3D dynamic programming model, on which the slice center and the radial lines number and length were adapted for each slice and an intern cost function between

adjacent slices was introduced. Based on this model, a slice by slice segmentation, starting from a middle slice and progressing to the two extremities is performed. This segmentation performs the transformation of each slice into an image composed by a series of equally spaced parallel vertical lines, transforming the nodules frontiers in horizontal curves. With this transformed image, the segmentation problem can be solved through the search of an optimal path with minimum cost using the dynamic programming algorithm. In the second stage, the segmented parts near to the nodule center are combined, for each direction, and an opening morphological operator is applied to obtain the final segmentation. To evaluate the proposed approach performance an overlap calculation was used to quantify the segmentation results consistency with the golden standard provided by the Lung Imaging Database Consortium [92].

Fuzzy

Lloréns et al. [116] propose a method for segmentation of jaw tissue in CT images. The presented method aims to reconstruct the jaw tissue starting from a set of serial cross-sections defined perpendicularly to the dental arch plane. The mandible is divided in 5 regions according to the tissue present on each region. The method scans each slice and estimates to which region each cross section belongs to and tries to segment the tissues present in the area. The hard tissues are segmented using a threshold technique associated with a boundary insertion in each cross-section. The boundaries are estimated through morphological operations. The nerve is segmented using Fuzzy Connectedness Object Extraction (FCOE), which is a method that starts with seed points and evaluate the affinity between seed and image pixel and, based on this affinity map and threshold, delimits the pixels that are connected to the same object. The seeds are extracted based on the pseudo-orthopantomographic projection and when all the cross-sections were segmented the 3D volume is reconstructed. Figure 7 shows the proposed algorithm flow. The method was tested on cross-sectional sets of 20 different patients, with their respective ground truth generated by a group of five experts, and the results were evaluated using 4 similarity measure (Jaccard index, Dice's coefficient, Point-to-point distance and Point-to-curve distance) showing their respective mean and also standard deviation values.

In [117], Ziyue Xu et al. present 3D segmentation algorithm to segment rib cage in chest CT scans. The approach has four steps: high-intensity bone structures segmentation; Multi-scale Hessian analysis; Detection of bone structures other than rib cage; and separation from detected structures from the rib cage. For high-intensity bone structures segmentation the fuzzy connectedness (FC) is employed. Then, Multi-scale Hessian analysis is performed to calculate the plateness and vesselness aiming to enhance the plate-like bones of sternum and scapula while excluding tubular ribs. In the detection of bone structures other than rib cage step, calculated plateness and vesselness information are employed. Lastly, for the separation from the detected structures from the rib cage, a thresholding, using the plateness and vesselness information, was applied to extract candidate plate voxels. Next, an iterative relative fuzzy connectedness (IRFC) method was used to finish removing voxels that belong to plate bone. This four steps result in the final rib cage segmentation. To evaluate the proposed algorithm performance the authors performed initially a visual qualitative evaluation of the rib cage segmentation results by two experts. Then, for a quantitative evaluation, 50 slices were selected and experts were asked to manually draw the separation curves between the rib cage and other bones on the overlapping whole bone segmentation. The Hausdorff distance, computed between the proposed method and the reference, was employed for quantification.

A method for kidney segmentation is presented by Hong Song et al. [118]. The proposed method employs a strategy of coarse-to-fine segmentation divided in two stages : rough and refined segmentation. Before the execution of these two stages, a median filter is applied to reduce the noise. In the rough stage, a kernel fuzzy C-means algorithm with spatial information (SKFCM) is used. Basically, the SKFCM introduces a kernel function and spatial constraint into the traditional FCM algorithm. In the refined stage, a improved GrowCut algorithm is used, which, differently from the GrowCut algorithm, can generate seed labels automatically. Lastly, a a post-processing method based on morphological

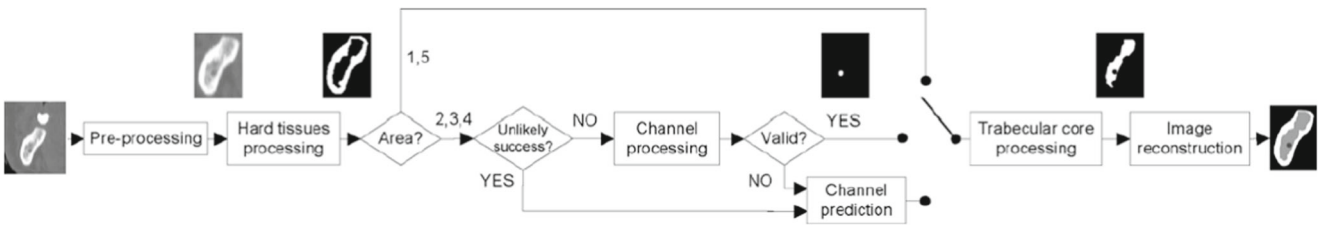

Fig. 7 Flow of the algorithm proposed by Lloréns. Extracted from [116]

operations is employed. The proposed method evaluation was conducted on three groups of abdominal CT images. The performance was assessed comparing the obtained results from the proposed method and the traditional method with a gold standard in terms of accuracy, overlap, the number of interactions (NOI) and the time of generating seed points by manual method or computer algorithm method (TOGSP). The method also was compared in terms of accuracy, sensitivity and specificity against other kidney segmentation methods.

In [119], Weidong Zhang et al. proposed a 3D segmentation method to segment the whole colon from a computed tomography colonography (CTC) data. The proposed method is basically composed of four steps: rough colon localization; initial 3D segmentation; colon tagged materials and non-colon regions classification; and final 3D segmentation generation. The rough colon localization and, posterior, initial 3D segmentation are performed using a pre-trained colon atlas probability map fit into the region of interest with anatomy constraints. The colon tagged materials and non-colon regions classification is performed by extracting features (2D and 3D Haar features) and generating a training set of positive and negative samples. Then, a cascade of Adaboost classifiers are adopted for feature selection and classification. Lastly, for the final 3D segmentation generation, the fuzzy-connectedness (FC) is used to segment the colon tagged material from the intersection to the colon wall. To evaluate the proposed method performance the false positive rate (FPR), volume overlap (VO) and Dice coefficient were employed, comparing the obtained results with ground truth generated by automated segmentation and slice by slice refinement performed by experts.

Geodesic Distance Segmentation

Yeonggul Jang et al. [120] present a method for 3D segmentation of the ascending aorta from coronary computed tomography angiography (CCTA). The method is composed by three steps: seed points selection, ascending aorta segmentation, seed points transfer. In the seed point selection, first the most probable ascending aorta circle among the axial-slices is found, using the circular Hough transform and a correlation between ascending and descending aortas. A volume of interest (VOI) is set based on the center and radius of the detected circle. In the ascending aorta segmentation step, the aorta in the detected circle is segmented by the geodesic distance algorithm in VOI over the axial slices, using the first segmented slice as basis for segmentation seeding for adjacent slices (seed point transfer step). The proposed method was evaluated by comparing the results with ground truths and a commercially available workstation in terms of Dice similarity coefficient.

Genetic Algorithms

Rusu et al. [121] describe a workflow to automatically segment filaments on cryon-electron tomography (cryo-ET) maps, which included all pre-segmentation part finalizing with the segmentation and result comparison. The pre-processing part is composed by the followings steps: The first step consist on the test and use of two noise removal filters, the Gaussian-weighted averaging and digital paths supervised variance. The second step is the normalization, aiming to improve the structure features appearance and equalize an uneven density distribution on the maps. The third step is the map edition, through the use of polygon clipping tools and flood fill algorithm with multiple points, aiming to assist on the regions without filaments removal. The next step is the image degradation correction, performing a mitigation dependent on the filaments intensity orientation. After the pre-processing part, the proper filament segmentation is performed using the volume trace (VolTrac), which employs a genetic algorithm for, initially, placing randomly cylindrical templates and, with the mutation and crossover processes, perform the search for the cylinders that maximize the fitness value. Lastly, the workflow is finalized with the result validation, comparing the obtained results for the automatic filaments segmentation with a manual segmentation performed by specialists.

Hessian Matrix Based

Gonçalves et al. [122] propose a method for lung nodule segmentation in CT images. The method uses a process of multiple-scale segmentation that employs the adaptive central medialness principle. This adaptive principle, consists in a strategy based on Hessian matrix, which provide a good segmentation in structures with particle shapes (blobs) as is the case on lung nodules. As the focus of the proposed work is the nodule segmentation, the strategy starts from a detected nodule localization aiming to evaluate the proposed method on the nodule volume extraction task. Therefore, initially, a multiple-scale smoothness filter is used to reduce the noise level. After that, the 3D Hessian matrix and its correspondent eigenvalues are computed and combined to generate the segmentation mask. In the combination for the mask generation, three approaches were tested. The first one, calculates the shape index and the curvedness from the biggest and the smallest Hessian matrix eigenvalues. The second, uses the two biggest eigenvalues to measure the structure force and their ratio is applied to correct the deviation from the target structure center. The third approach, uses a combination of the two previously presented approaches through the union of the detection provided by each one. After the structure

enhancement, where nodules can be clearly identified, the last step is the threshold application to select voxels with a high response and, therefore, build the masks by the final nodule segmentation connectivity. The different approaches were evaluated in different lung nodule cases present in the LIDC [92] database. Each tomographic volume used was evaluated by four radiologists and only nodules that had a strong consensus between the specialists were considered. The Jaccard index was used as comparison measure between the proposed approaches and the manual segmentation ground truth performed by human specialists.

Histogram Based

Fabijanska et al. [123] propose a method for segmentation of regions filled with the cerebrospinal fluid in brain CT images. The method consists of the following steps: Initially, the user indicates a seed with ellipsoidal shape within the ROI. Then, the input data is normalized to the range of intensities varying from $[0, 255]$, highlighting values corresponding to cerebral tissues and attenuating values corresponding to the surrounding air and the dense tissue. Next, a histogram H_{sd} that represents the voxel intensity within the ellipsoidal region previously informed as seed is calculated. This reference histogram is compared with the local distribution intensity across the image in order to identify voxels belonging to the segmented object. In the fourth step, the local histogram H_{xy} in a circular neighborhood is collected for each voxel in the same plane and a similarity map between local histogram and the reference histogram is calculated through the Bhattacharyya distance, assigning a similarity level for each voxel. To improve the brain desired region accuracy detection, the similarity map is enhanced with the application of an intensity reconstruction followed by morphological opening with an appropriate ellipsoid structuring element. Lastly, a thresholding method (OTSU) is applied on the similarity map to produce the final segmentation. The proposed method accuracy was measured through the DICE similarity coefficient and the Jaccard index in five cases of brain CT images.

Isosurface Manipulation

X. Wan et al. [124] present method which integrates the segmentation and visualization together to generate meaningful visualization results of multiple anatomical structures. The method can be divided in three stages: feature locating, structure extracting, and structure recombining. In the feature locating stage, the objective is to identify and visualize a specific feature of interest, e.g., whole organ or a segment of an organ. Two process are executed in this stage: appropriate isosurface selection (containing the structure) and undesired structures removal. The isosurface selection can be performed by the isovalue tuning and the cropping and peeling operations are used to remove undesirable structures. In the structure extracting stage, after locating the feature it is possible that the feature is not completely isolated; thus, to extract the structure of interest, an interactive segmentation procedure is employed. The segmentation procedure consists on the selection of foreground and background voxels, in the isosurface, that are used as seeds. This seeds are used to perform a min-cut based optimization procedure to decide a geometrically shortest cut that divides the two sets of seeds. This two stages can be applied to each structure of interest and the results can be recombined to generate a multi-valued mask volume in the structure recombining stage. The proposed method was tested in a thorax computed tomography angiography dataset to extract the kidneys and the heart. It was also tested in an ear CT dataset, where the surgeon is interested in a couple of different structures, i.e., the cochlea, the facial nerve, and the chorda.

Polynomial Fitting

Biesdorf et al. [125] proposed a new approach for blood vessel segmentation in computed tomography angiography (CTA) images. This approach uses a local implicit polynomial fitting and a convex optimization combined with an incremental tracking scheme. The proposed method can be summarized on three main steps: initialization, local model parameter estimation, and tracking along the vessel centerline. In the initialization part, a coarse estimation is required for the starting point, the local orientation, and the ROI radius for model fitting. These information are needed only for the first vessel segment initialization, for the other vessel segments the previous vessel segmentation result is used. For the local model parameters estimation, the convex objective function is minimized in a 3D ROI around a vessel. For minimization, a projected gradient descent approach is used and the parameter update is computed iteratively. For the tracking along the vessel centerline, a new 3D position is predicted based on the estimate centerline position and on the local 3D current vessel segment orientation. The proposed approach was tested in more than 100 synthetic images and in 10 different CTA clinical images, measuring the approach accuracy based on relevant clinical parameters (minimum, mean, and maximum vessel diameter) as well as the mean error for the centerline position and the mean Dice similarity coefficient.

Tree Bagger Classifier

The work proposed by Farzaneh et al. [126] present a method for 3D segmentation of convexity subdural

hematomas in head CT images. The method initially performs the skull segmentation and tissue intensity normalization based on intensity parameters. Then, to find the intracranial region where the convexity SDHs occur, first the region contained by the skull has to be segmented. If there is no fracture or the skull is closed, this process is resumed to segment the area enclosed by the skull. Otherwise, a customized version of the distance regularized level set evolution (DRLSE) method is used to find the brain border. After the ROI definition, a feature extraction process is performed extracting statistical, textural, and geometrical information. These features are used to classify each voxel as hematoma or non-hematoma by means of a Tree Bagger Classifier. After the classification process, a 3D post-processing method is applied to 3D representation of the binary classification result to reduce the number of false positives. The results obtained with the proposed method were compared with a gold standard, calculating the sensitivity and specificity similarity values and generating the ROC curve for evaluation.

Template Matching

The work proposed by Czabaj et al. [127] combines imaging, visualization, and numerical reconstruction of a fiber-reinforced polymer in a 3D X-ray computed tomography microscope images. The polymer under study is the graphite/epoxy and the first step is the digitization on submicron resolution. For a correct numerical reconstruction, a segmentation algorithm is used to identify and estimate correctly the individual fiber positioning in the volume. The segmentation algorithm employed is divided in two steps: in the first step, a template-matching (TM) algorithm is used to detect 2D coordinates of individual fiber centroids in each cross-sectional image of the volume. Each template selection was performed through the trial and error. In the second step, the multi-fiber assignment and tracking algorithm uses the TM detection part to determine the 3D coordinate for each individual fiber in the volume. After the fiber segmentation, an algorithm to convert the resulting segmentation data (coordinate and diameters) into a detailed 3D finite element mesh of the composite is used. The described algorithm was applied to sub-volumes of size 169^3 and evaluated qualitatively, based on the reconstruction visualization, and quantitatively based on the fibers distribution and on the fiber's angles computation, which measures misorientation of any given fiber relative to the global Z-Axis.

Tensor Voting

An approach for segmentation and quantification of object filaments in 3D electron tomography images is proposed by Loss et al. [128]. This approach consists of three steps: The first step is the use of a Hessian filter for local filaments enhancement; The second step is the detection and completion of filamentous structures through tensor voting; The third step is the filamentous networks delineation through 3D tracking curves algorithm, which allows the detection and labeling of filaments. The tracking curve algorithm iterates between finding voxels to be used as seed, for tracking, and linking adjacent voxels along a consistent direction. The proposed method was initially evaluated in synthetic data with noise insertion and for its quantitative evaluation two variables were computed (precision and recall). In other experiment, real cell wall samples that suffer different chemical treatments were used, aiming to quantify the plants cell walls compositional and morphometric properties. This experiment results were validated and compared against previously published works.

Swarm Intelligence

An approach for segmentation of structures in 3D and 2D images, using specification of the bacterium colony segmentation (BCS) technique, is presented by Pawel Badura [129]. This new swarm intelligence optimization technique, represented in Fig. 8, is a heuristic tool provided for certain parts of segmentation methods. The method starts with the initialization of colony members and preparation of any auxiliary data. The main loop is composed by five steps: bacteria movements; calculation of new bacteria velocities; deposition of pheromone trails; pheromone evaporation; and bacteria sizes modification. This loop is executed until a break condition is reached, using the pheromone distribution to produce the binary segmentation result. The experiments performed with the proposed method employed several image types (2D and 3D synthetic and CT images, CAD domains and 2D ultrasonography) and the results were validated using sensitivity and Dice index metrics of spacial overlap.

Several Algorithms

This section report works that have more than one segmentation method being analyzed such as surveys and comparative studies.

The work proposed by Ontiverosa et al. [130], for example, performs an analysis of edge detection techniques for application in metrology in CT images. Initially, the author explains each of the common techniques used for edge detection (Atlas-guided, deformable models, detection of discontinuities, pattern classification, region-oriented, threshold-based, trainable segmentation, Watershed transformation) making reference to some methods for each technique. Then, the author select two methods, justifying the specific selection of these two and not the others,

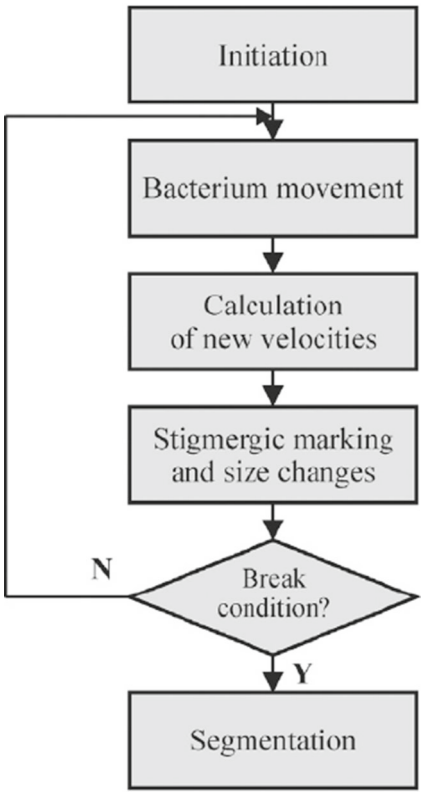

Fig. 8 Scheme of the BCS segmentation algorithm. Extracted from [129]

detailed in Fig. 9. The two selected methods, threshold and canny, were used in a comparative analysis through their application on a reference volume. In this evaluation, both methods were applied more then 10 times, comparing the measures differences related to the model volume previously calibrated. The comparison analysis results showed the canny method repeatability power and the local threshold higher accuracy and lower repeatability rate, indicating the possibility of the canny method being more corrected than the threshold.

The work presented by Rudyanto et al. [131] shows algorithms for automated vessel segmentation, aiming to provide a platform to compare the segmentation algorithms performance in lung vessel identification process applied to CT images. A reference dataset containing annotations about 20 CTs and the proposal of nine categories to perform evaluation was elaborated. The developed study has all the description about the data set acquisition (pathology, image type, scanner and kernel, spacing, number of slices, voltage, and amperage), the definition of evaluation categories, the presented segmentation method categorization (author, image type, if it is multi-scale or not and if it has a pre-processing step) and all the score part with the results statistical analysis. Based on the presented work, the author claims that its main contribution are: the reference dataset containing annotations, the quantitative system for scoring and the segmentation methods comparison and evaluation, highlighting the strong and weak points of each of them in the presence of some lung diseases.

The next work was proposed by Valente et al. [132] and presents a survey based on methods for automatic identification of lung nodules in CT images. The performed study shows the methodology used that goes from the selection criterion for published works to a critical analysis about them and the future prospects for the study area. The works selected for evaluation were categorized according to presence or not of the five principal stages, normally presented on diagnostic aid systems. The five principal stages are: (i) data acquisition, (ii) pre-processing, (iii) lung segmentation, (iv) nodule detection, and (v) false positives reduction. For each stage, there is a description about their operation with the most used techniques and, for some of these steps, a table is presented showing specifically the method used by each work. In the survey is also described a comparative table with the author's name and the presence or not of some features considered important for each work individually. Some of these important features are the method sensitivity, the number of false positive per exam, the number of nodules used on the validation process, the nodules size, the execution time, and the nodule type. Lastly, the author makes a summary about the automatic nodule identification area actual stage, based on the analyzed works.

Performance Evaluation Analysis

One important aspect for the development of 3D segmentation algorithms is its evaluation. To perform such evaluation, the analyzed works focused on specific aspects such as robustness, specificity, sensitivity, accuracy, precision, recall, and others. Those aspects were measured, in general, based on the number of false positives, false negatives, true positives, and true negatives. Some of the analyzed works used a qualitative evaluation associated with the quantitative analysis and some used only qualitative evaluation. For the qualitative evaluation, in the analyzed works' scope, the subjective analysis was predominant, e.g., visual analysis of the obtained results; however, it is not commonly used for a wide comparison between segmentation algorithms. In general, the evaluation is performed based on the specialist knowledge, i.e., the obtained segmentation results are compared to a manually performed segmentation, normally called by the names of ground-truths, golden pattern, or golden standard, employing a specific metric or specific characteristics for evaluation.

On the analyzed works that had a qualitative analysis, the metrics most used were the DICE similarity coefficient

Methods	Information used	Training	Computational cost	Comments
Atlas-guides	Spatial map	Yes	Low	It was not selected because it is necessary an atlas construction.
Deformable models	Feature vector	No	Medium	It was not selected due to the heavily dependence of the results on the manual interaction to place an initial model and choose appropriate parameters.
Detection of discontinuities	Voxel	No	Medium	**It was selected because provides a good surface location capability and significantly reduces the data quantity.**
Pattern classification	Feature vector	Yes	Medium	It was not selected because its main goal is just distinguish image features, also can be sensitive to noise and intensity in-homogeneities.
Region oriented	Image patch	No	Low	It was not selected because requires manual interaction to obtain the seed point that must be planted, also segmentation can be sensitive to noise, partial volume effects can cause separate regions to become connected.
Threshold based	Voxel	No	Low	**It was selected because it is stable in images with different structures; also there are some works that have been carried out for metrology applications.**
Trainable segmentation	Feature vector	Yes	High	It was not selected because they learn by example and has a high computational cost.
Watershed transformation	Image patch	No	Low	It was not selected because this segmentation method generally leads to over-segmentation due to noise and local irregularities of the gradient.

Fig. 9 Table with the methods analyzed by Ontiverosa. Extracted from [130]

[133], the Jaccard index [134], and the commonly used specificity, accuracy and sensitivity. Some works employed custom metrics, but those were, in general, related to the golden standard or an atlas. Herng-Hua Chang et al. [135] present a detailed analysis of performance measures for evaluation of neuroimage segmentation algorithms, where DICE coefficient, Jaccard index, specificity, accuracy, sensitivity, and other metrics such as Anderberg, Blanque and Kulczynsk are further explained in their brain image context. Although the authors present those metrics for the brain images segmentation context, still the metrics concepts and use are the same when compared with other image types (2D images, computed tomography from several areas and so on). Other metrics for 3D segmentation method evaluation can be found on the work proposed by Taha et al. [136]. In [136], 19 3D image segmentation metrics were implemented in a tool used for validation. The author presents a table with the 19 metrics referencing their definition and articles that use the metric in medical images, as well as a detailed analysis of those metrics.

Discussion

From a systematic point of view, we can highlight some key aspects about 3D segmentation applied to tomographic images:

- The use of 3D segmentation algorithms based on CT images is still focused in the Human Healthy area, as showed on the chart Fig. 10. However, there are some areas demonstrating a growing tendency for 3D segmentation as well, e.g., geology and general objects.
- There is a vast amount of 3D segmentation techniques with different methodologies applied, which indicates a constant and growing research in the 3D segmentation area.
- The histogram, indicated in Fig. 11, shows the main methods grouped according to its frequency occurrences. From this graph, one can notice that the model-based methods are the most used in the covered period, which indicates that the use of models to guide the segmentation process, in the 3D segmentation scope, has obtained more positive results. Also, we notice that the threshold methods were used with a lower frequency. However, this category of methods are frequently presented in several analyzed works as supporting or as an initialization procedure for other methods, demonstrating the importance of such technique.

Also, we can point out that the proposed review, following the Kitchenham's methodology, demonstrates (i) a reproducible search with a systematic methodology to review 3D segmentation algorithms applied to tomographic images on the period from 2006 to march of 2018. Figure 12 shows the analyzed works frequency by publication year; (ii) a summary of all the analyzed works that match with the established criteria, specifying the main segmentation method, the image type used, the experiments performed, and the performance evaluation methods employed by each work, categorizing each work into its respective groups; (iii)

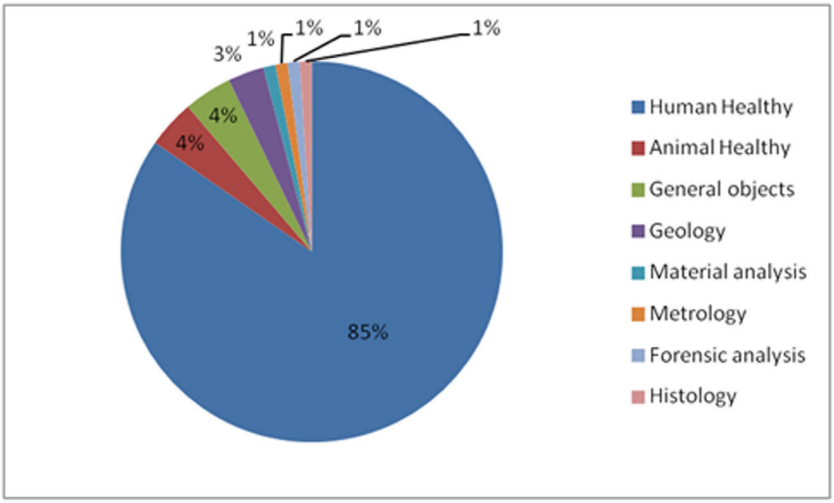

Fig. 10 Pizza chart showing the frequency of the main application areas, based on the analyzed works

a general overview analyzing, based on the selected works, the 3D segmentation area with application in tomographic images.

Limitations

In our review, some limitations aspects are present and mainly refer to the systematic methodology procedure. The systematic methodology key aspect of turning the search reproducible, when the same key words and tags are used, also produce a closed scope limited by the keywords, tags and search strings employed. In our case, we limited our review to 3D segmentation algorithms applied to tomographic images. Thus, 3D segmentation algorithms applied to other image modality would not be contemplated in our review. Also, we delimited the year range from 2006 to March 2018; thus, works published outside this range were not evaluated. Another important step of the systematic methodology is the exclusion criterion application. In our review, we excluded works that were not available for analysis, i.e., we did not have access to the complete work. Additionally, we excluded works that were not written in English and that only employed the segmentation method, i.e., used a software for the segmentation procedure; thus, the segmentation method was not the main procedure being evaluated in some application area.

Future Prospects

Based on the gathered information provided from the analyzed works, it can be observed that 3D segmentation methods (newer or existing ones) must take performance aspects into account in order to obtain results with some degree of efficiency. Real parallel execution is still explored in a very subtle manner, opening a wide opportunity for further research and development. Qualitatively speaking, a unified methodology for evaluation is still required, once the

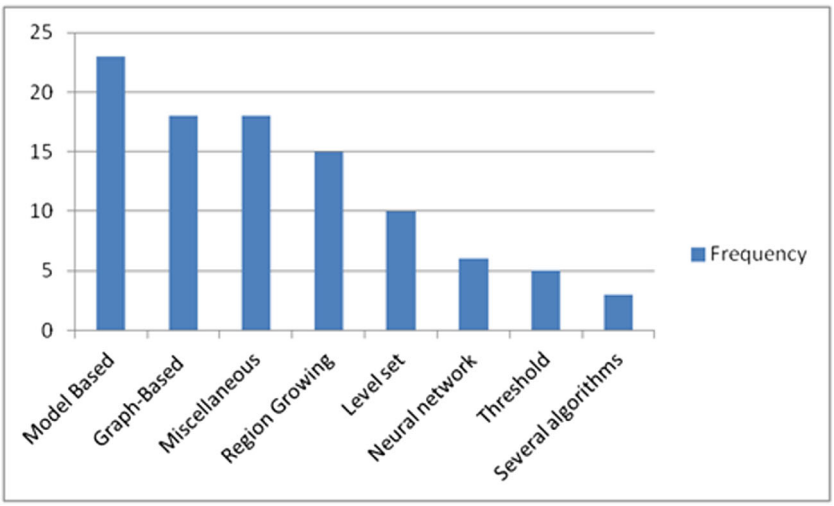

Fig. 11 Histogram showing the frequency of the main method used based on the analyzed works grouping

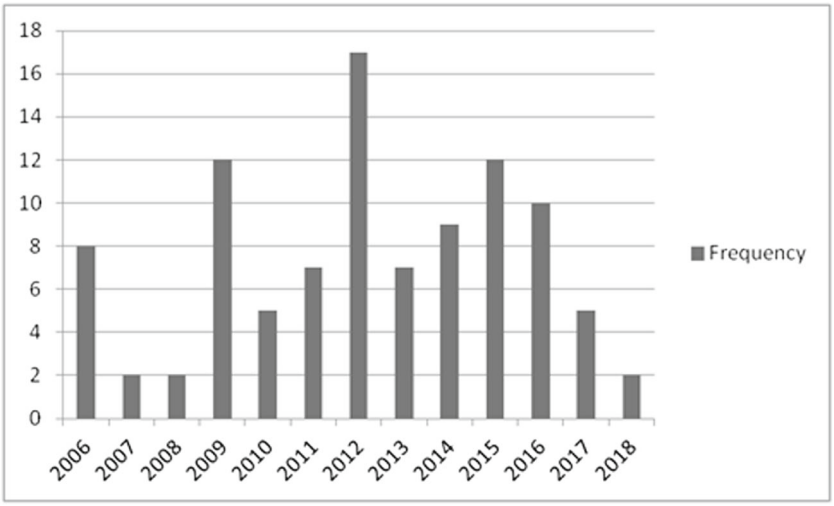

Fig. 12 Histogram showing the frequency of the analyzed works by year of publication.

arose methodologies use proper datasets whose images were acquired under very controlled conditions and generally, if not publicly available, cannot be reproduced and used as a comparison benchmark for other segmentation methods. Also, we can make some assumptions of the future direction that the 3D segmentation area, applied to tomographic images, is taking:

- an increase on the use of hybrid segmentation methods, i.e., methods that use more than one type of segmentation, seeking to produce more reliable results;
- employment of 3D segmentation methods in more areas than Human Healthy area, driven by a large popularization of 3D sensors;
- development of parallel segmentation methods, boosted by the increase on the quantity of information available and the GPU and multi-core processors development;
- validation and evaluation methodologies appearance, providing a more unified form for segmentation methods comparison;
- use of large datasets for 3D segmentation algorithms evaluation;
- extension and application of 2D segmentation methods that still were not evolved for 3D.

Conclusion

This systematic literature review presented a general overview regarding 3D segmentation area applied to tomographic images. The research included articles published between 2006 and March 2018 on Science Direct, IEEEXplore, ACM, and PubMed. Advances in qualitative and quantitative evaluation and application in areas other than the Human Healthy area, were demonstrated, but there are still areas to be tested and methodologies to be formalized.

In general, several published studies showed their potential in the Human Healthy area, however, the presented method generalization power is still an open question. An experiment testing this power would be a possible experiment to compare the methods abilities in several areas other than the medical one. This experiment would only be possible through a joint effort between the authors, to formalize a methodology for validation and evaluation in a specific framework, which would test all the methods in the same illumination, clutter, and resolution conditions, which are constant problems in the segmentation area.

This review with the methods analysis, performed experiments, performance evaluation analysis, and future prospects, is useful for researches working with tomographic images that require a full 3D segmentation method application for better image understanding and discretization.

References

1. Gonzalez RC, Woods RE: Digital image processing, 2nd edition. Upper Saddle River: Prentice-Hall, Inc., 2006
2. Ilea DE, Whelan PF: Image segmentation based on the integration of colour-texture descriptors- a review. Pattern Recogn 44(10-11):2479–2501, 2011. Semi-Supervised Learning for Visual Content Analysis and Understanding
3. Ma Z, Tavares J, Jorge RN: A review on the current segmentation algorithms for medical images, 2009, pp 135–140, 01
4. Ma Z, Tavares JMRS, Jorge RM, Mascarenhas TR: Natal a review of algorithms for medical image segmentation and their applications to the female pelvic cavity. Comput Methods Biomech Biomed Eng 13(2):235–46, 2010
5. Jodas DS, Pereira AS, Tavares JMRS: A review of computational methods applied for identification and quantification of atherosclerotic plaques in images. Expert Syst Appl 46:1–14, 2016
6. Kitchenham B: Procedures for Performing Systematic Reviews. Technical report Joint Technical Report TR/SE-0401, 2004

7. National Health, Medical Research Council (Australia), and Nhmrc Staff. How to Review the Evidence: Systematic Identification and Review of the Scientific Literature. Handbook series on preparing clinical practice guidelines. National Health and Medical Research Council, 2000
8. National Health, Medical Research Council (Australia), and Nhmrc Staff. How to Use the Evidence: Assessment and Application of Scientific Evidence. Handbook series on preparing clinical practice guidelines. National Health and Medical Research Council, 2000
9. Cochrane Collaboration. Cochrane Reviewers Handbook. Version 4.2.1. National Health and Medical Research Council, 2003
10. University of York. NHS Centre for Reviews and Dissemination. Undertaking systematic reviews of research on effectiveness: CRD's guidance for those carrying out or commissioning reviews. CRD report. NHS Centre for Reviews and Dissemination, University of York, 2001
11. Katz YH: Automatic pattern recognition of meteorological satellite cloud photography, 1964
12. Joan SW: A survey of threshold selection techniques. Comput Graph Image Process 7(2):259–265, 1978
13. Li Z, Lee K, Niemeijer M, Mullins RF, Sonka M, Abramoff MD: Automated segmentation of the choroid from clinical sd-oct. Investig Ophthalmol Vis Sci 53(12):7510–7519, 2012
14. Javaid M, Javid M, Rehman MZU, Shah SIA: A novel approach to {CAD} system for the detection of lung nodules in {CT} images. Comput Methods Programs Biomed 135:125–139, 2016
15. Armato SG, McLennan Gx, Bidaut L, McNitt-Gray MF, Meyer CR, Reeves AP, Zhao B, Aberle DR, Henschke CI, Hoffman EA, et al: The lung image database consortium (lidc) and image database resource initiative (idri): a completed reference database of lung nodules on ct scans. Med Phys 38(2):915–931, 2011
16. Chang KY, Wu YH, Lin WL, Chen SJ, Chen LS: Vessel segmentation based on bone-to-bone elimination in brain ct angiography. In 2016 IEEE International Conference on Consumer Electronics-Taiwan (ICCE-TW), 2016, pp 1–2
17. Migliori S, Chiastra C, Bologna M, Montin E, Dubini G, Aurigemma C, Fedele R, Burzotta F, Mainardi L, Migliavacca F: A framework for computational fluid dynamic analyses of patient-specific stented coronary arteries from optical coherence tomography images. Med Eng Phys 47:105–116, 2017
18. Farzaneh N, Habbo-Gavin S, Soroushmehr SMR, Patel H, Fessell DP, Ward KR, Najarian K: Atlas based 3d liver segmentation using adaptive thresholding and superpixel approaches. In: 2017 IEEE International Conference on Acoustics,Speech and Signal Processing (ICASSP), 2017, pp 1093–1097
19. Boykov Y, Veksler O, Zabih R: Markov random fields with efficient approximations. In: Proceedings of the IEEE Computer Society Conference on Computer Vision and Pattern Recognition, CVPR '98. IEEE Computer Society, Washington, 1998, p 648
20. Yi F, Moon I: Image segmentation: a survey of graph-cut methods. In: 2012 International Conference on Systems and Informatics (ICSAI), 2012, pp 1936–1941
21. Wieclawek W, Pietka E: Live-wire-based 3d segmentation method. In: 2007 29th Annual International Conference of the IEEE Engineering in Medicine and Biology Society, 2007, pp 5645–5648
22. Liu J, Udupa JK, Saha PK, Odhner D, Hirsch BE, Siegler S, Simon S, Winkelstein BA: Rigid model-based 3d segmentation of the bones of joints in mr and ct images for motion analysis. Med Phys 35(8):3637–3649, 2008
23. Aslan MS, Ali A, Arnold B, Fahmi R, Farag AA, Xiang P: Segmentation of trabecular bones from vertebral bodies in volumetric ct spine images. In: 2009 16th IEEE International Conference on Image Processing (ICIP), 2009, pp 3385–3388
24. Aslan MS, Ali A, Rara H, Arnold B, Fahmi R, Farag AA, Xiang P: A novel, fast, and complete 3d segmentation of vertebral bones. In: 2010 IEEE International Conference on Acoustics, Speech and Signal Processing, 2010, pp 654–657
25. Lu K, Higgins WE: Segmentation of the central-chest lymph nodes in 3d {MDCT} images. Comput Biol Med 41(9):780–789, 2011
26. Liu X, Tuncali K, Wells WM, Morrison PR, Zientara GP: Fully automatic 3d segmentation of iceball for image-guided cryoablation. In: 2012 Annual International Conference of the IEEE Engineering in Medicine and Biology Society, 2012, pp 2327–2330
27. Boykov Y, Kolmogorov V: An experimental comparison of min-cut/max- flow algorithms for energy minimization in vision. IEEE Trans Pattern Anal Mach Intell 26(9):1124–1137, 2004
28. Beichel R, Bornik A, Bauer C, Sorantin E: Liver segmentation in contrast enhanced ct data using graph cuts and interactive 3d segmentation refinement methods. Med Phys 39(3):1361–1373, 2012
29. Beichel RR, Wang Y: Computer-aided lymph node segmentation in volumetric ct data. Med Phys 39(9):5419–5428, 2012
30. Chen X, Niemeijer M, Zhang L, Lee K, Abramoff MD, Sonka M: 3D segmentation of fluid-associated abnormalities in retinal oct Probability constrained graph-search-graph-cut. IEEE Trans Med Imaging 31(8):1521–1531, 2012
31. Pazokifard B, Sowmya A: 3-d segmentation of human sternum in lung mdct images. In: 2013 35th Annual International Conference of the IEEE Engineering in Medicine and Biology Society (EMBC), 2013, pp 3351–3354
32. Grosgeorge D, Petitjean C, Dubray B, Su R: Esophagus segmentation from 3d ct data using skeleton prior-based graph cut. Computational and mathematical methods in medicine, 2013
33. El-Zehiry N, Jolly MP, Sofka M: A splice-guided data driven interactive editing. In: 2013 IEEE 10th International Symposium on Biomedical Imaging, 2013, pp 1098–1101
34. Antony BJ, Miri MS, Abràmoff MD, Kwon YH, Garvin MK, Howe R: Automated 3d segmentation of multiple surfaces with a shared hole: Segmentation of the neural canal opening in sd-oct volumes. In: Golland P, Hata N, Barillot C, Hornegger J Eds. Medical Image Computing and Computer-Assisted Intervention – MICCAI 2014. Springer International Publishing, Cham, 2014, pp 739–746
35. Jodoin PM, Pinheiro F, Oudot A, Lalande A: Left-ventricle segmentation of spect images of rats. IEEE Trans Biomed Eng 62(9):2260–2268, 2015
36. Vasquez D, Scharcanski J, Wong A: Automatic framework for extraction and characterization of wetting front propagation using tomographic image sequences of water infiltrated soils. PLOS ONE 01(1):1–12, 2015
37. Kitrungrotsakul T, Chen Y-W, Han X-H, Lin L: Supervoxels based graph cut for medical organ segmentation. IFAC-PapersOnLine 48(20):70–75, 2015. 9th {IFAC} Symposium on Biological and Medical Systems {BMS} 2015Berlin, Germany, 31 August-2 September 2015
38. Gangsei LE, Kongsro J: Automatic segmentation of computed tomography (ct) images of domestic pig skeleton using a 3d expansion of dijkstra's algorithm. Comput Electron Agric 121:191–194, 2016
39. Cha JW, Farhangi MM, Dunlap N, Amini A: Volumetric analysis of respiratory gated whole lung and liver ct data with motion-constrained graph cuts segmentation. In: 2017 39th Annual International Conference of the IEEE Engineering in Medicine and Biology Society (EMBC), 2017, pp 3405–3408
40. Osher S, Sethian JA: Fronts propagating with curvature dependent speed: algorithms based on hamilton-jacobi formulations. J Comput Phys 79(1):12–49, 1988

41. Burger M, Osher SJ: A survey on level set methods for inverse problems and optimal design, 2004
42. Liu J-W, Feng H-Q, Zhou Y-Y, LI C-F: A novel automatic extraction method of lung texture tree from {HRCT} images. Acta Autom Sin 35(4):345–349, 2009
43. Chen D, Fahmi R, Farag AA, Falk RL, Dryden, GW: Accurate and fast 3d colon segmentation in ct colonography. In: 2009 IEEE International Symposium on Biomedical Imaging: From Nano to Macro, 2009, pp 490–493
44. Chen D, Farag AA, Falk RL, Dryden, GW: A variational framework for 3d colonic polyp visualization in virtual colonoscopy. In: 2009 16th IEEE International Conference on Image Processing (ICIP), 2009, pp 2617–2620
45. Hadjiiski L, Mukherji SK, Ibrahim M, Sahiner B, Gujar SK, Moyer J, Chan H-P: Head and neck cancers on ct: preliminary study of treatment response assessment based on computerized volume analysis. Amer J Roentgenol 194(4):1083–1089, 2010
46. Hadjiiski L, Mukherji SK, Gujar SK, Sahiner B, Ibrahim M, Street E, Moyer J, Worden FP, Chan H-P: Treatment response assessment of head and neck cancers on ct using computerized volume analysis. Amer J Neuroradiol 31(9):1744–1751, 2010
47. Hadjiiski L, Weizer AZ, Alva A, Caoili EM, Cohan RH, Cha K, Chan H-P: Treatment response assessment for bladder cancer on ct based on computerized volume analysis, world health organization criteria, and recist. Amer J Roentgenol 205(2):348–352, 2015
48. Hutter J, Hofmann HG, Grimm R, Greiser A, Saake M, Hornegger J, Dörfler A, Schmitt P: Prior-based automatic segmentation of the carotid artery lumen in tof mra (pascal) Berlin: Springer, 2012, pp 511–518
49. Qi Y, Dong K, Yin L, Li M: 3d segmentation of the lung based on the neighbor information and curvature. In: Proceedings of the 2013 Seventh International Conference on Image and Graphics, ICIG '13. IEEE Computer Society, Washington, 2013, pp 139–143
50. Hemmati H, Kamli-Asl A, Talebpour A, Shirani S: Semi-automatic 3d segmentation of carotid lumen in contrast-enhanced computed tomography angiography images. Phys Med 31(8):1098–1104, 2015
51. Badura P, Wieclawek W: Calibrating level set approach by granular computing in computed tomography abdominal organs segmentation. Appl Soft Comput 49(C):887–900, 2016
52. IRCAD France. 3dircadb, 3d image reconstruction for comparison of algorithm database, Available from: http://www.ircad.fr/research/3d-ircadb-01/. Accessed 19.04.18
53. Suetens P, Verbeeck R, Delaere D, Nuyts J, Bijnens (Auth.) B, Stefanelli M, Hasman A, Fieschi M, Talmon J: AIME 91: Proceedings of the Third Conference on Artificial Intelligence in Medicine, Maastricht, June 24-27, Lecture Notes in Medical Informatics, vol 44, 1st edition. Berlin: Springer, 1991
54. Geman S, Geman D: Stochastic relaxation, gibbs distributions, and the bayesian restoration of images. IEEE Trans Pattern Anal Mach Intell PAMI-6(6):721–741, 1984
55. Huang, Rui, Pavlovic V, Metaxas DN: A tightly coupled region-shape framework for 3d medical image segmentation. In: 3rd IEEE International Symposium on Biomedical Imaging: Nano to Macro, 2006, pp 426–429
56. Juslin A, Tohka, J: Unsupervised segmentation of cardiac pet transmission images for automatic heart volume extraction. In: 2006 International Conference of the IEEE Engineering in Medicine and Biology Society, 2006, pp 1077–1080
57. Müller O, Donner S, Klinder T, Dragon R, Bartsch I, Witte F, Krüger A, Heisterkamp A, Rosenhahn B: Model based 3d segmentation and oct image undistortion of percutaneous implants. In: Proceedings of the 14th International Conference on Medical Image Computing and Computer-assisted Intervention - Volume Part III, MICCAI'11. Springer, Berlin, 2011, pp 454–462
58. Bhole C, Morsillo N, Pal C: 3d segmentation in ct imagery with conditional random fields and histograms of oriented gradients. In: Proceedings of the Second International Conference on Machine Learning in Medical Imaging, MLMI'11. Springer, Berlin, 2011, pp 326–334
59. Mesejo P, Ibánez Ó, Cordón Ó, Cagnoni S: A survey on image segmentation using metaheuristic-based deformable models: state of the art and critical analysis. Appl Soft Comput 44:1–29, 2016
60. Terzopoulos D, Fleischer K: Deformable models. Vis Comput 4(6):306–331, 1988. cited By 392
61. Saragaglia A, Fetita C, Prêteux F: Assessment of airway remodeling in asthma: Volumetric versus surface quantification approaches. In: Proceedings of the 9th International Conference on Medical Image Computing and Computer-Assisted Intervention - Volume Part II, MICCAI'06. Springer, Berlin, 2006, pp 413–420
62. Zhang H, Yang L, Foran DJ, Nosher JL, Yim PJ: 3d segmentation of the liver using free-form deformation based on boosting and deformation gradients. In: Proceedings of the Sixth IEEE International Conference on Symposium on Biomedical Imaging: From Nano to Macro, ISBI'09. IEEE Press, Piscataway, 2009, pp 494–497
63. Ding, F, Yang W, Leow WK, Venkatesh SK: 3d segmentation of soft organs by flipping-free mesh deformation. In: 2009 Workshop on Applications of Computer Vision (WACV), 2009, pp 1–7
64. Cascio D, Magro R, Fauci F, Iacomi M, Raso G: Automatic detection of lung nodules in ct datasets based on stable 3d mass-spring models. Comput Biol Med 42(11):1098–1109, 2012
65. Delibasis KK, Christodoulidis A, Maglogiannis I: An intelligent tool for anatomical object segmentation using deformable surfaces. In: Proceedings of the 7th Hellenic Conference on Artificial Intelligence: Theories and Applications, SETN'12. Springer, Berlin, 2012, pp 206–213
66. Shi C, Guo C, Cheng Y, Wang J: Greedy algorithm based deformable simplex meshes using gradient vector flow as external energy. In: 2014 7th International Conference on Biomedical Engineering and Informatics, 2014, pp 199–204
67. Lu D, Wu Y, Harris G, Cai W: Iterative mesh transformation for 3d segmentation of livers with cancers in ct images. Comput Med Imaging Graph 43:1–14, 2015
68. Kass M, Witkin A, Terzopoulos D: Snakes: active contour models. Int J Comput Vis 1(4):321–331, 1988
69. Jiang H, Cheng Q: Automatic 3d segmentation of ct images based on active contour models. In: 11th IEEE International Conference on Computer-Aided Design and Computer Graphics, 2009. CAD/graphics '09, 2009, pp 540–543
70. Barbosa D, Dietenbeck T, Schaerer J, D'hooge J, Friboulet D, Bernard O: B-spline explicit surfaces: active an efficient framework for real-time 3-d region-based segmentation. IEEE Trans Image Process 21(1):241–251, 2012
71. Qi D, Angelini ED, Laine AF: Real-time segmentation by active geometric functions. Comput Methods Prog Biomed 98(3):223–230, 2010
72. Urschler M, Bornik A, Scheurer E, Yen K, Bischof H, Schmalstieg D: Forensic-case analysis: from 3d imaging to interactive visualization. IEEE Comput Graph Appl 32(4):79–87, 2012
73. Mezlini H, Youssef R, Bouhadoun H, Budyn E, Denis Laredo J, Ghalila SS, Chappard C: High resolution volume quantification of the knee joint space based on a semi-automatic segmentation of computed tomography images. In: 2015 International

Conference on Systems, Signals and Image Processing (IWSSIP), 2015, pp 157–161
74. Akkus Z, Sedlar J, Coufalova L, Korfiatis P, Kline TL, Warner JD, Agrawal J, Erickson BJ: Semi-automated segmentation of pre-operative low grade gliomas in magnetic resonance imaging. Cancer Imaging 15(1):12, 2015
75. Heimann T, Meinzer H-P: Statistical shape models for 3d medical image segmentation A review. Med Image Anal 13(4):543–563, 2009
76. Cootes TF, Taylor CJ, Cooper DH, Graham J: Training Models of Shape from Sets of Examples London: Springer, 1992, pp 9–18
77. Nain D, Haker S, Bobick A, Tannenbaum A Shape-driven 3d segmentation using spherical wavelets. In: International Conference on Medical Image Computing and Computer-Assisted Intervention. Springer, 2006, pp 66–74
78. Moussavi F, Heitz G, Amat F, Comolli LR, Koller D, Horowitz M: 3d segmentation of cell boundaries from whole cell cryogenic electron tomography volumes. J Struct Biol 170(1):134–145, 2010
79. Badakhshannoory H, Saeedi P: A model-based validation scheme for organ segmentation in ct scan volumes. IEEE Trans Biomed Eng 58(9):2681–2693, 2011
80. Zhang S: Towards Robust and Effective Shape Prior Modeling: Sparse Shape Composition. New Brunswick: PhD thesis 2012, AAI3502515
81. Zhang S, Huang J, Uzunbas M, Shen T, Delis F, Huang X, Volkow N, Thanos P, Metaxas DN: 3d segmentation of rodent brain structures using hierarchical shape priors and deformable models. In: International Conference on Medical Image Computing and Computer-Assisted Intervention. Springer, 2011, pp 611–618
82. Rüegsegger MB, Cuadra Meritxell B, Pica A, Amstutz CA, Rudolph T, Aebersold D, Kowal JH: Statistical modeling of the eye for multimodal treatment planning for external beam radiation therapy of intraocular tumors. Int J Radiat Oncol*Biol*Phys 84(4):e541–e547, 2012
83. Chang Y-B, Xia JJ, Yuan P, Kuo T-H, Xiong Z, Gateno J, Zhou X: 3d segmentation of maxilla in cone-beam computed tomography imaging using base invariant wavelet active shape model on customized two-manifold topology. J X-ray Sci Technol 21(2):251–282, 2013
84. Brice CR, Fennema CL: Scene analysis using regions. Artif Intell 1(3):205–226, 1970
85. Haralick RM, Shapiro LG: Image segmentation techniques. Comput Vis Graph Image Process 29(1):100–132, 1985
86. Freixenet J, Muñoz X, Raba D, Martí J, Cufí X: Yet another survey on image segmentation: Region and boundary information integration. In: Proceedings of the 7th European Conference on Computer Vision-Part III, ECCV '02. Springer, London, 2002, pp 408–422
87. Bernard Davis J, Reiner B, Huser M, Burger C, Székely G, Frank Ciernik I: Assessment of 18f {PET} signals for automatic target volume definition in radiotherapy treatment planning. Radiother Oncol 80(1):43–50, 2006
88. Staal J, van Ginneken B, Viergever MA: Automatic rib segmentation and labeling in computed tomography scans using a general framework for detection, recognition and segmentation of objects in volumetric data. Med Image Anal 11(1):35–46, 2007
89. Monga O: Defining and computing stable representations of volume shapes from discrete trace using volume primitives: Application to 3d image analysis in soil science. Image Vis Comput 25(7):1134–1153, 2007
90. Bulu H, Alpkocak A: Comparison of 3d segmentation algorithms for medical imaging. In: Twentieth IEEE International Symposium on Computer-Based Medical Systems (CBMS'07), June 2007, pp 269–274
91. Diciotti S, Picozzi G, Falchini M, Mascalchi M, Villari N, Valli G: 3-d segmentation algorithm of small lung nodules in spiral ct images. IEEE Trans Inf Technol Biomed 12(1):7–19, 2008
92. Armato SG, McLennan G, Bidaut L, McNitt-Gray MF, Meyer CR, Reeves AP, Zhao B, Aberle DR, Henschke CI, Hoffman EA, Kazerooni EA, MacMahon H, Beek EJR, Yankelevitz D, Biancardi AM, Bland PH, Brown MS, Engelmann RM, Laderach GE, Max D, Pais RC, Qing DP-Y, Roberts RY, Smith AR, Starkey A, Batra P, Caligiuri P, Farooqi A, Gladish GW, Matilda Jude C, Munden RF, Petkovska I, Quint LE, Schwartz LH, Sundaram B, Dodd LE, Fenimore C, Gur D, Petrick N, Freymann J, Kirby J, Hughes B, Casteele AV, Gupte S, Sallam M, Heath MD, Kuhn MH, Dharaiya E, Burns R, Fryd DS, Salganicoff M, Anand V, Shreter U, Vastagh S, Croft BY, Clarke LP: The lung image database consortium (lidc) and image database resource initiative (idri): a completed reference database of lung nodules on ct scans. Med Phys 38(2):915–931, 2011
93. Lai K, Zhao P, Huang Y, Liu J, Wang C, Feng H, Li C: Automatic 3d segmentation of lung airway tree A novel adaptive region growing approach. In: 2009 3rd International Conference on Bioinformatics and Biomedical Engineering, 2009, pp 1–4
94. De Nunzio G, Tommasi E, Agrusti A, Cataldo R, De Mitri I, Favetta M, Maglio S, Massafra A, Quarta M, Torsello M, Zecca I, Bellotti R, Tangaro S, Calvini P, Camarlinghi N, Falaschi F, Cerello P, Oliva P: Automatic lung segmentation in ct images with accurate handling of the hilar region. J Digit Imaging 24(1):11–27, 2011
95. Bert A, Dmitriev I, Agliozzo S, Pietrosemoli N, Mandelkern M, Gallo T, Regge D: An automatic method for colon segmentation in {CT} colonography. Comput Med Imaging Graph 33(4):325–331, 2009
96. Gloger O, Kühn J, Stanski A, Völzke H, Puls R: A fully automatic three-step liver segmentation method on lda-based probability maps for multiple contrast {MR} images. Magn Reson Imaging 28(6):882–897, 2010
97. Ren Yh, Sun Xw, Nie Sd: A 3d segmentation method of lung parenchyma based on ct image sequences. In: International Conference on Information, Networking and Automation (ICINA), vol 2, 2010, pp V2–332–V2–336
98. Uher V, Burget R: Automatic 3d segmentation of human brain images using data-mining techniques. In: 2012 35th International Conference on Telecommunications and Signal Processing (TSP), 2012, pp 578–580
99. Andrä H, Combaret N, Dvorkin J, Glatt E, Han J, Kabel M, Keehm Y, Krzikalla F, Lee M, Madonna C, Marsh M, Mukerji T, Saenger EH, Sain R, Saxena N, Ricker S, Wiegmann A, Zhan X: Digital rock physics benchmarks-part i: Imaging and segmentation. Comput Geosci 50:25–32, 2013. Benchmark problems, datasets and methodologies for the computational geosciences
100. Badura P, Pietka E: Soft computing approach to 3d lung nodule segmentation in {CT}. Comput Biol Med 53:230–243, 2014
101. Werz T, Baumann M, Wolfram U, Krill I CE: Particle tracking during ostwald ripening using time-resolved laboratory x-ray microtomography. Mater Charact 90:185–195, 2014
102. Paulano F, Jiménez JJ, Pulido R: 3d segmentation and labeling of fractured bone from ct images. Vis Comput 30(6-8):939–948, 2014
103. Pal NR, Pal SK: A review on image segmentation techniques. Pattern Recogn 26(9):1277–1294, 1993
104. Blanz WE, Gish SL: A connectionist classifier architecture applied to image segmentation. In: [1990] Proceedings, 10th International Conference on Pattern Recognition, volume ii, 1990, pp 272–277

105. Amza, C: A review on neural network–based image segmentation techniques. De Montfort University, Mechanical and Manufacturing Engg, The gateway leicester, LE1 9BH, United Kingdom, 2012, pp 1–23
106. Li S, Fevens T, Krzyźak A, Li S: Automatic clinical image segmentation using pathological modeling, {PCA} and {SVM}. Eng Appl Artif Intell 19(4):403 – 410, 2006. Recent Advances in Data Mining
107. Chang Q, Shi J, Xiao Z: A new 3d segmentation algorithm based on 3d pcnn for lung ct slices. In: 2009 2nd International Conference on Biomedical Engineering and Informatics, 2009, pp 1–5
108. Santos AM, de Carvalho Filho AO, Silva AC, de Paiva AC, Nunes RA, Gattass M: Automatic detection of small lung nodules in 3d {CT} data using gaussian mixture models, tsallis entropy and {SVM}. Eng Appl Artif Intell 36:27–39, 2014
109. Ye ZZ, Yu QZ, Liao M, Zou BJ, Wang XF, Wang W: Liver vessel segmentation based on extreme learning machine. Phys Med 32(5):709–716, 2016
110. Wang S, Mu Z, Liu Z, Liu Z, Gu D, Zang Y, Di D, Gevaert O, Tian J: Central focused convolutional neural networks: Developing a data-driven model for lung nodule segmentation. Med Image Anal 40:172–183, 2017
111. Gibson E, Li W, Sudre C, Fidon L, Shakir DI, Wang G, Eaton-Rosen Z, Gray R, Doel T, Hu Y, Whyntie T, Nachev P, Modat M, Barratt DC, Ourselin S, Jorge Cardoso M, Vercauteren T: Niftynet: a deep-learning platform for medical imaging. Comput Methods Programs Biomed 158:113–122, 2018
112. Chaves R, Ramírez J, Górriz JM: Integrating discretization and association rule-based classification for alzheimer's disease diagnosis. Expert Syst Appl 40(5):1571–1578, 2013
113. Spampinato C, Pino C, Giordano D, Leonardi R: Automatic 3d segmentation of mandible for assessment of facial asymmetry. In: 2012 IEEE International Symposium on Medical Measurements and Applications Proceedings (MeMeA), 2012, pp 1–4
114. Karvonen T, Uranishi Y, Sakamoto T, Tona Y, Okamoto K, Tamura H, Kuroda T: 3d reconstruction of cochlea using optical coherence tomography. In: 2016 38th Annual International Conference of the IEEE Engineering in Medicine and Biology Society (EMBC), 2016, pp 5905–5908
115. Wang Q, Song E, Jin R, Han P, Wang X, Zhou Y, Zeng J: Segmentation of lung nodules in computed tomography images using dynamic programming and multidirection fusion techniques1. Acad Radiol 16(6):678–688, 2009
116. Lloréns R, Naranjo V, López F, Alcaniz M: Jaw tissues segmentation in dental 3d {CT} images using fuzzy-connectedness and morphological processing. Comput Methods Programs Biomed 108(2):832–843, 2012
117. Xu Z, Bagci U, Jonsson C, Jain S, Mollura DJ: Efficient ribcage segmentation from ct scans using shape features. In: 2014 36th Annual International Conference of the IEEE Engineering in Medicine and Biology Society, 2014, pp 2899–2902
118. Song H, Kang W, Zhang Q, Wang S: Kidney segmentation in ct sequences using skfcm and improved growcut algorithm. BMC Syst Biol 9:1–11, 2015
119. Zhang W, Kim HM: Fully automatic colon segmentation in computed tomography colonography. In: 2016 IEEE International Conference on Signal and Image Processing (ICSIP), 2016, pp 51–55
120. Jang Y, Ho YJ, Hong Y, Cho I, Shim H, Chang H: Geodesic distance algorithm for extracting the ascending aorta from 3d CT images. Comp Math Methods Med 2016:4561979:1–4561979:7, 2016
121. Rusu M, Starosolski Z, Wahle M, Rigort A, Wriggers W: Automated tracing of filaments in 3d electron tomography reconstructions using sculptor and situs. J Struct Biol 178(2):121–128, 2012. Special Issue: Electron Tomography
122. Gonçalves L, Novo J, Campilho A: Hessian based approaches for 3d lung nodule segmentation. Expert Syst Appl 61:1–15, 2016
123. Fabijańska A, Goclawski J: 3d segmentation of the cerebrospinal fluid from ct brain scans using local histogram similarity map. In: 2015 IEEE 2nd International Conference on Cybernetics (CYBCONF), 2015, pp 113–118
124. Wan X, Yang F, Yang F, Li X, Xu M, Tian J: Visualization of multiple anatomical structures with explicit isosurface manipulation. In: 2015 37th Annual International Conference of the IEEE Engineering in Medicine and Biology Society (EMBC), 2015, pp 4234–4237
125. Biesdorf A, Wörz S, von Tengg-Kobligk H, Rohr K, Schnörr C: 3d segmentation of vessels by incremental implicit polynomial fitting and convex optimization. In: 2015 IEEE 12th International Symposium on Biomedical Imaging (ISBI), 2015, pp 1540–1543
126. Farzaneh N, Soroushmehr SMR, Williamson CA, Jiang C, Srinivasan A, Bapuraj JR, Ward KR, Korley FK, Najarian K: Automated subdural hematoma segmentation for traumatic brain injured (tbi) patients. In: 2017 39th Annual International Conference of the IEEE Engineering in Medicine and Biology Society (EMBC), 2017, pp 3069–3072
127. Czabaj MW, Riccio ML, Whitacre WW: Numerical reconstruction of graphite/epoxy composite microstructure based on sub-micron resolution x-ray computed tomography. Compos Sci Technol 105:174–182, 2014
128. Loss LA, Bebis G, Chang H, Auer M, Sarkar P, Parvin B: Automatic segmentation and quantification of filamentous structures in electron tomography New York: ACM, 2012, pp 170–177
129. Badura P: Virtual bacterium colony in 3d image segmentation. Comput Med Imaging Graph 65:152–166, 2018. Advances in Biomedical Image Processing
130. Ontiveros S, Yagüe JA, Jiménez R, Brosed F: Computer tomography 3d edge detection comparative for metrology applications. Procedia Eng 63:710 – 719, 2013. The Manufacturing Engineering Society International Conference {MESIC}
131. Rudyanto RD, Kerkstra S, van Rikxoort EM, Fetita C, Brillet P-Y, Lefevre C, Xue W, Zhu X, Liang J, Öksüz Í, Ünay D, Kadipasaog˘lu K, San josé estépar R, Ross JC, Washko GR, Prieto J-C, Hoyos MH, Orkisz M, Meine H, Hüllebrand M, Stö cker C, Mir Fernando L, Naranjo V, Villanueva E, Staring M, Xiao C, Stoel BC, Fabijanska Aa, Smistad Erik, Elster AC, Lindseth F, Foruzan AH, Kiros R, Popuri K, Cobzas D, Jimenez-Carretero D, Santos A, Ledesma-Carbayo MJ, Helmberger M, Urschler M, Pienn M, Bosboom DGH, Campo A, Prokop M, de Jong Pim A, de Solorzano CO, Barrutia AM, van Ginneken B: Comparing algorithms for automated vessel segmentation in computed tomography scans of the lung: the {VESSEL12} study. Med Image Anal 18(7):1217–1232, 2014
132. Valente IRS, Cortez PC, Neto EC, Soares JM, de Albuquerque VHC, Tavares JMRS: Automatic 3d pulmonary nodule detection in ct images. Comput Methods Prog Biomed 124(C):91–107, 2016
133. Dice LR: Measures of the amount of ecologic association between species. Ecology 26(3):297–302, 1945
134. Ben-Hur A, Elisseeff A, Guyon I: A stability based method for discovering structure in clustered data Pacific Symposium on Biocomputing Pacific Symposium on Biocomputing, 2002, pp 6–17
135. Chang H-H, Zhuang AH, Valentino DJ, Chu W-C: Performance measure characterization for evaluating neuroimage segmentation algorithms. NeuroImage 47(1):122–135, 2009
136. Taha AA, Hanbury A: Metrics for evaluating 3d medical image segmentation: analysis, selection, and tool. BMC Med Imaging 15(1):29, 2015